STUDYING AN ALL-VANADIUM PHOTOELECTROCHEMICAL CELL FOR HIGHLY EFFICIENT SOLAR ENERGY CONVERSION AND STORAGE VIA PHOTOCATALYTIC REDOX REACTION

by

DONG LIU

Presented to the Faculty of the Graduate School of

The University of Texas at Arlington in Partial Fulfillment

of the Requirements

for the Degree of

DOCTOR OF PHILOSOPHY

THE UNIVERSITY OF TEXAS AT ARLINGTON

AUGUST 2015

Acknowledgements

They all say that this is one of the most important sections in one's PhD thesis, I could not agree more as this is where readers get to know the author personally.

Except those hardships I had and sacrifice I made in last five years, the state of my mind toward the future life through this PhD training is way more influential than the training itself. For that, I am very very grateful! To this end, I like to express my sincere thanks firstly to my supervisor Dr. Fuqiang Liu. I would not be able to complete this program without his continuous encouragement, knowledge, technical help and financial support in last five years. Not only did he work with me closely on things we have little knowledge or experience of from the scratch, but also he taught me ways to conduct carefully designed, analytically meticulous and logically rigorous research. Most important, he is the only person who let me feel that I am actually doing something great for the first time in my whole academic life combined. It is such a privilege to ever be one of his students!

Secondly, I would like to thank my committee members Dr. Krishnan Rajeshwar, Dr. Efstathios "Stathis" Meletis, Dr. Weidong Zhou, Dr. Yaowu Hao, Dr. Kyungsuk Yum, and Dr. Harry F. Tibbals for their valuable comments, suggestions and criticisms during my comprehensive and dissertation defense. My parents always told me to be grateful for those who sound harsh during my study, so special thanks go to Dr. Rajeshwar for his critical but beneficial criticism to help me stay on the right track of this research.

In addition, I sincerely appreciate the scientific discussion, perspective, criticism, technical aid and mental support from all of my past and current lab mates, Dr. Noor Siddique, Dr. Chiajen Hsu, Dr. Mingsheng Wei, Wei Zi, Syed Dawar Sajjad, Yi Shen, Snigdha Rajendra Rashinkar, Shambhavi Raju Sakri, Amir Hosein Salehi Gilani, Sonam Patel for my research through which we made very good friends and colleagues. They

created a very friendly and professional work environment in our lab. Among them, Zi worked with me on this research very closely and her contribution to this research is one of the reason I can go this far. She and Dr. Noor Siddique are much more than just a colleague for their kindness, patience, endurance, encouragement and trust to me all the time!

Furthermore, I also need to express the gratitude to the Characterization Center for Materials and Biology (CCMB) in my department for providing me instrument trainings. Since vast characterization work needs to be done in the research, I would not imagine this possible without this well-maintained center and its facilities by the lab manager Dr. Jiechao Jiang and lab technician David Yan.

All faculty members from Department of Materials Science and Engineering have taught me comprehensive and useful courses within the program, I say thank you to all of them by heart regardless of my future professional career pathway. All past and current department staffs, Beth Robinson, Jennifer Standlee and Libia Cuauhtli are also praised for offering me generous help.

Meanwhile, my friends, Manouchehr Teimouri, Jain, Astha, Vibhu Sharma, Kush Shah, Felipe Monte, Ami, Shah, Gaurav Nagalia, Akshay Hande, Orathai Thumthan, Randle Kelton, Derek Wong, Yishu Wang, Minghui Zhang, Jacky Lu, Kunhua Yu, Aaron Chiu, Ruiqian Jiang, Yang Li, Golsa Mortazavi, Vinay Sharma, Sunil Sahi, Cheng Sheng, Shuye Wang, Wenbo Zhu, Fuqiang Zhang, Hongzhu Liao, Yuetao Sun, Cancan Xu, Xiaosong Duan, Dr. Fangcheng Xu, Dr. Lei Qiao, Dr. Xueyang Cheng, Dr. Chengdong Xu, Dr. Nan Zhang, Dr. Wei Li, Dr. Jun Zhou, Dr. Ye Zhou and their company in last five years are appreciated!

Last but not the least, I am indefinitely indebted to all my family. My wife is the most beautiful, elegant, considerate and amazing woman I have ever seen. Her endless

faith, support, inspiration, trust and love for me constitutes the cornerstone behind this degree. My son is one of the greatest gift I have received from HIM and his birth completes this family. My parents especially my mother upheld their son since he was 18 to travel thousands of miles within the country and even across the ocean to pursue his dream, I cannot even begin to imagine the enormous sacrifice, faith, trust and love they had for me. For that, I am grateful forever! My parents-in-law and their great encouragement, support and love are also one of the reasons this challenge becomes much easier.

I apologize to those who accompanied and helped me and whose name I forgot to mention in this acknowledgement.

July 14, 2015

Abstract

STUDYING AN ALL-VANADIUM PHOTOELECTROCHEMICAL CELL FOR HIGHLY EFFICIENT SOLAR ENERGY CONVERSION AND STORAGE VIA PHOTOCATALYTIC REDOX REACTION

Dong Liu, PhD

The University of Texas at Arlington, 2015

Supervising Professor: Fuqiang Liu

This study aims at developing a promising alternative approach to utilize solar energy continuously with high efficiency by employing photocatalytic vanadium redox reactions to overcome major drawbacks associated with conventional photoelectrochemical water splitting.

The preliminary study was implemented on TiO_2 and WO_3/TiO_2 by linear sweep voltammetry (LSV), cyclic voltammetry (CV) and zero-resistance ammetry (ZRA) in a photoelectrochemical cell (PEC). The results show much enhanced photoelectrochemical response with the assistance of vanadium(IV, VO^{2+}) redox species. Such photoresponse improvement is attributed to the hole scavenging effect by fast vanadium redox reaction to depress charge recombination at semiconductor/liquid interface in both TiO_2 and WO_3/TiO_2 cases. Facilitated electron transfer from WO_3 to TiO_2 further contributes to the photoresponse of WO_3/TiO_2 hybrid electrode due to their band structures interplay.

During the study, a unique photocharging/discharging process was discovered and modeled on WO_3-based hybrid electrodes due to the formation/decomposition of hydrogen tungsten bronze (H_xWO_3) from WO_3 under AM 1.5 illumination in highly acidic environment. Comparison of electrochemical impedance spectroscopy (EIS) results on

TiO_2 and WO_3/TiO_2 electrodes indicates that vanadium redox species, due to their fast electrochemical kinetics, not only enhance the photocurrents under illumination, but also help release reversely the stored electrons under dark through decomposition reaction of H_xWO_3.

To further improve photocatalytic property of the PEC, the conventional H_2SO_4 was replaced with a novel supporting electrolyte, methanesulfonic acid (MSA) as a simple but feasible optimization measure. CV, zero-resistance ammetry (ZRA) and conductivity measurements demonstrate its excellent chemical stability, high conductivity and superior photoelectrochemical performance over H_2SO_4, especially when vanadium redox species were involved in the electrolyte. The root cause of such ability of MSA relies on its prolonged electron lifetime and being capable of dramatically diminishing charge transfer resistance and interfacial capacitance at photoelectrode/electrolyte interface under AM1.5 illumination, according to EIS Nyquist plot and Bode plot results.

To quantify the efficiency of proposed all-vanadium PEC, the Faradaic efficiency and Incident photon-to-electron conversion efficiency of the cell were measured. While the Faradaic efficiency of the cell reaches to 84.8% after a 60-h cell operation, the IPCE of the cell was improved on V-MSA by a factor of 18.6, 9.7 and 2.5 compared to pure H_2SO_4, V-H_2SO_4 and pure MSA respectively. Such remarkable IPCE enhancement of the cell is believed due to synergy between fast vanadium redox kinetics and prolonged electron life time of MSA.

Table of Contents

List of Illustrations

List of Tables

Nomenclature

Abbreviation	Meaning
PEC	photoelectrochemcical cell
PV	photovoltaic
PESC	photoelectrochemical storage cell
SCR	space charge region
HER	hydrogen evolution reaction
OER	oxygen evolution reaction
STH	solar-to-hydrogen
VRB	vanadium redox battery
CVD	chemical vapor deposition
PLD	pulsed laser deposition
PVD	physical vapor deposition
CB	conduction band
VB	valence band
LSV	linear cyclic voltammetry
CV	cyclic voltammetry
ZRA	zero-resistance ammetry
EIS	electrochemical impedance spectroscopy
WE	working electrode
CE	counter electrode
RE	reference electrode
NHE	normal hydrogen electrode
XRD	x-ray diffraction
SEM	scanning electron microscope
EDS	Energy-dispersive x-ray spectroscopy
JCPDS	joint committee on powder diffraction standards
MSA	methanesulfonic acid
IPCE	incident photon-to-current conversion efficiency

CHAPTER 1

Introduction

Solar energy, including radiant light and heat from the sun, has been harnessed by humans since ancient times using a range of ever-evolving technologies. These technologies include indirect methods using meteorological or geophysical effects, or direct methods as use of solar energy in the form of heat, generation of electric power by photovoltaic process and storage the solar energy by converting it to chemical fuels.[1, 2] The indisputable fact that more energy from sunlight strikes earth in 1 hour than all the energy consumed by humans in an entire year is the sole driving force for mankind to promote wider and deeper utilization of solar energy.[2, 3]

Among those generic methods mentioned above to utilize solar energy, three approaches, natural photosynthesis, photoelectrochemical cell (PEC) and photovoltaic (PV) cell are known for producing storable energy from sunlight as demonstrated in Figure 1-1.[4] Natural photosynthesis in plants relies on solar energy to convert carbon dioxide (CO_2) and water (H_2O) to oxygen (O_2) and glucose (a source of fuel) with a conversion efficiency of about 3%. The PEC transforms the sun's energy into an electrical current, or a chemical fuel, such as hydrogen (H_2), from a liquid such as water. The most effective PECs can produce chemical fuels with a conversion efficiency of about 10% and electricity with an efficiency of about 16% while PV cells convert light to electricity with an efficiency as high as 25% even back in 90's.[4] With its high energy conversion efficiency and the development of semiconductors, mainly Si, photovoltaic cell or solar cell, as a potentially widespread approach to sustainable energy production, is receiving heightened attention. This is because increased economical, environmental and ecological concerns toward carbon-neutral energy production have been seriously taken by human beings. So far, the solar cells have been the dominating devices in which the

junction is formed between inorganic solid-state materials, usually doped forms of crystalline or amorphous silicon, which development has benefited from the experience and material availability in the semiconductor industry.[5]

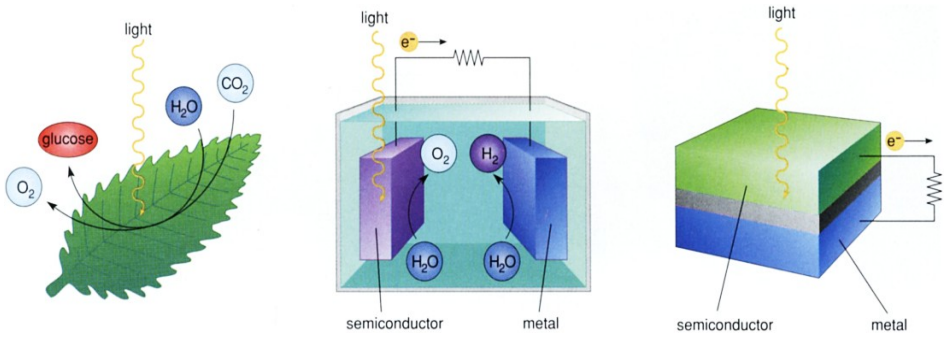

Figure 1-1 Three approaches known for storing solar energy: Natural photosynthesis (left), PEC (middle), and PV (right).

However, the inorganic solid-state junction solar cell faces new challenges in the coming years mainly due to material-to-device manufacturing cost.[2] For example, the sale price of grid-connected PV electricity must excel a $0.25-0.30 per kilowatt-hour (kWh) threshold to recover the initial capital investment and cost over the lifetime of the PV operation for a practical PV module with efficiency of 15-20%. The demand for producing cost-effective PV module is crucial in every level. Another key issue hurdling scalable implementation of PV technology lies in the trade-off between material purity and device performance.[2] In a typical planar solar cell design, the charge carriers are collected in the same direction as light is absorbed. A minimum thickness of the cell is set by the thickness of material required to absorb >90% of the incident sunlight. However, the required thickness of the material also imposes a constraint on the required purity of the material, because the photogenerated charge carriers must live sufficiently long enough within the absorbing material to arrive at the electrical junction, where they can be separated to produce an electrical current flow through the metallic contacts to the

cell. In other words, impure absorber materials with short charge carrier lifetimes can effectively absorb sunlight but cannot convert it effectively. On the contrary, absorber materials with the necessary purity are generally costly to produce and manufacture. This cost-thickness-purity constraint, combined with expensive manufacturing cost is largely the cause why all current PV cells are incomparable to utility-scale power generation approaches.[2, 3]

Table 1-1 Comparison between semiconductor-liquid junction photoelectrochemical cells with solid state junction solar cells.

	Solid state photo-voltaic solar cells	Semiconductor-liquid junction photoelectro-chemical solar cells
1. Material synthesis	Costly	Relatively cheap
2. Material tailoring	Costly	Relatively cheap
3. Junction formation	Difficult	Relatively easy
4. Routine conversion efficiency	High 10% (≥20% in special devices)	Moderate (>7% in special Dye-sensitized cells)
5. *In situ* storage	Not possible	Possible
6. Stability of cell	Stable	Stability has been achieved through proper modification of the electrolyte solution
7. Economic viability	Viable, but ~ 10× cost of conventional electricity	Viable, one order cheaper than solid state solar cells

Due to the continuing, rapid worldwide progress in nano-science/technology and photoelectrochemistry, a new category of solar energy utilization, photoelectrochemical cell, has been invented featuring a solid-liquid junction formed between the semiconductor and the electrolyte interface. In contrast to solid state photovoltaic devices, semiconductor/liquid junction based photoelectrochemical cells are relatively

inexpensive involving convenient and economically viable material synthesis and tailoring processes, and are easy to fabricate. The semiconductor/liquid configuration offers the following four advantages:[3] (1) the junction required for efficient charge separation of photogenerated electrons and holes is very easily formed by simply immersing the semiconductor in an appropriate electrolyte solution; (2) the liquid electrolyte offers the capability of a readily conformable and strain-free junction; (3) a third electrode can be added to PEC cells to provide in-situ chemical storage for 24 hr/day power; and (4) the conversion of solar energy directly into fuel eliminates the need for external wires and a separate electrolyzer. The PEC approach to solar energy conversion has achieved high efficiencies for both electrical power (>15%) and hydrogen generation (>10%) to date. Compared to solid-state junction solar cells, the most important and vital advantage given in Table 1-1 in PECs is the possibility of *in situ* storage[3, 6] because PECs naturally offer the opportunity to integrate the energy conversion and storage functions.

PEC has been shown to directly split water into H_2 and O_2, thereby providing a promising basis for the renewable, clean production of hydrogen from sunlight. The materials can be cheap polycrystalline forms, because of the relaxed requirements on the minority carrier diffusion length. However, the known materials, which are robust in water splitting, are not responsive to a wide portion of the solar radiation spectrum; they work best in the ultraviolet (UV) region- yielding relatively low solar-to-electrical (STE) efficiencies. Finding new photoelectrodes, either individually or in combination, that can allow the efficient, integrated conversion of sunlight to chemical fuels, is one of the primary aims of solar energy conversion research. The goal is to identify PEC systems that display the same efficiency and stability for visible-light-induced water splitting as those demonstrated for near-UV-light-induced water splitting.[3] Closing this gap will lead to the development of cheap and efficient systems that, in an integrated fashion, could

produce chemical fuels (e.g., H_2) directly from sunlight and therefore directly address, not only the conversion, but also the storage issues, associated with solar energy conversion schemes.

This Ph.D. dissertation primarily focused on the three major challenges that have hindered the development of efficient solar energy storage using PECs in the past, i.e., continuous energy conversion (despite the intermittent nature of sunlight), high capacity energy storage medium, and reversible conversion reaction kinetics. This research strives to establish a methodology for the systematic design and effective integration of high efficiency regenerative solar energy storage using all vanadium redox species, as an alternative to photoproduction of H_2. Most important, a tandem WO_3/TiO_2photoelectrode was designed to effectively tune the photogenerated charge flow, so that the electrons could be stored in the photoelectrode upon solar illumination and released under dark, allowing potentially uninterrupted solar energy conversion.

Chapter 2

Background Information and Objective of the Study

2.1 Introduction

The discovery by Fujishima and Honda[7] in 1972 offered the prospect of using sunlight to produce environmentally-friendly fuel. However, the critical hurdle preventing its wide-spread implementation is hydrogen handling. Although molecular hydrogen has very high energy density on a mass basis, as a gas at ambient conditions it has very low energy density by volume. Pressurization and liquefaction increase volumetric density, but also bring inconvenience and safety concerns. Moreover, sluggish kinetics of photoelectrolysis of water and gas evolution reactions requires a large electrochemical overpotential, which contributes to a low efficiency.

In this chapter, the fundamental basics of photoelectrochemical solar water splitting along with its current challenges are reviewed. To overcome these challenges, alternative approaches to more efficiently utilize sunlight such as photoelectrochemical solar energy conversion and storage are introduced briefly. Among them, redox reaction-assisted solar energy conversion and storage are considered one promising method to achieve high efficiency, low-cost and non-intermittent solar energy utilization. At last, the scope of this study and description of this dissertation are elaborated in details.

2.2 Operating Principles of the PEC

The principle of operating a typical PEC has been constantly reviewed in many literatures[5, 8-12] and also explained in Figure 2-1. In general, photons of energy exceeding that of the semiconductor bandgap (E_g) generate electron–hole pairs, which are intrinsically separated by the electric field present in a very thin layer of the semiconductor (called space charge region, SCR) at the interface. Under the influence of the electrical field, the negative charge carriers move through the bulk of the n-type

semiconductor to the current collector and then to the external circuit. The positive holes are driven to the surface where they are scavenged by a redox species (R) to its oxidized form (O). The oxidized form O is reduced back to R on the counter electrode by the electrons that re-enter the cell from the external circuit. This type of PEC is called regenerative cell that converts light to electric power leaving no net chemical change behind but heat. However, if the redox species is water, water will be cleaved by sunlight, or photoelectrolysis, as water is oxidized by holes to oxygen at the semiconductor photoelectrode and reduced by electrons to hydrogen at the other electrode. Because of this promising merit, water-splitting by PEC is considered to be the most cost-effective renewable approach for hydrogen production.[3, 5, 13]

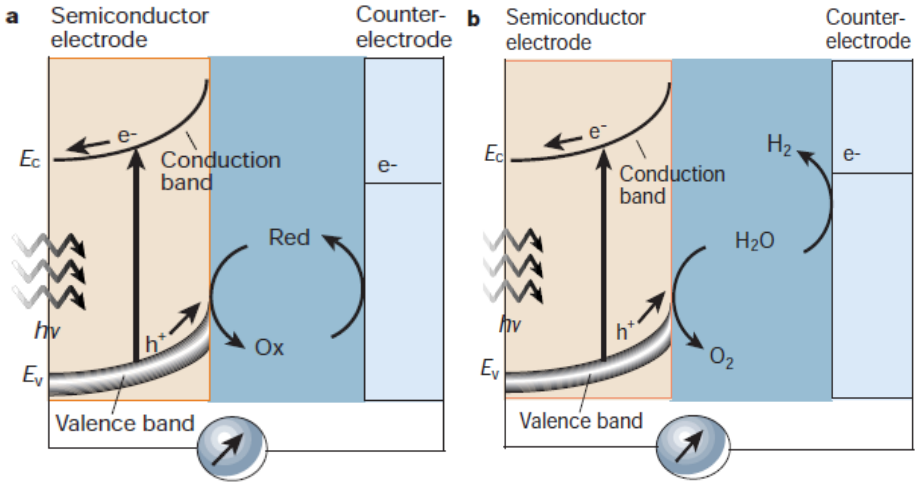

Figure 2-1 Operation principle of photoelectrochemical cells based on n-type semiconductor. a) Regenerative-type cell producing electric current from sunlight; b) A cell that generates a chemical fuel, hydrogen, through the photo-cleavage of water.

2.3 Photoelectrochemical Water Splitting

The free energy change for the conversion of one molecule of H_2O to H_2 and 1/2 O_2 under standard conditions is ΔG= 237.2 kJ/mol, which, according to the Nernst

equation, corresponds to ΔE°=1.23 V per electron transferred. To use a semiconductor and drive this reaction with light, the semiconductor must absorb radiant light with photon energy >1.23 eV (equal to wavelengths of ~1000 nm and shorter) and convert the energy into H_2 and O_2. This process must generate two electron-hole pairs per molecule of H_2.[12, 13] Thermodynamically, a semiconductor must have a band gap energy (Eg) large enough to split water, and a conduction band-edge energy (E_{cb}) and valence band-edge energy (E_{vb}) that straddle the electrochemical potentials of E° (H^+/H_2) and E° (O_2/H_2O), to drive the hydrogen evolution reaction (HER) and oxygen evolution reaction (OER) using the electrons/holes generated under illumination.

2.3.1 Thermodynamic Requirement

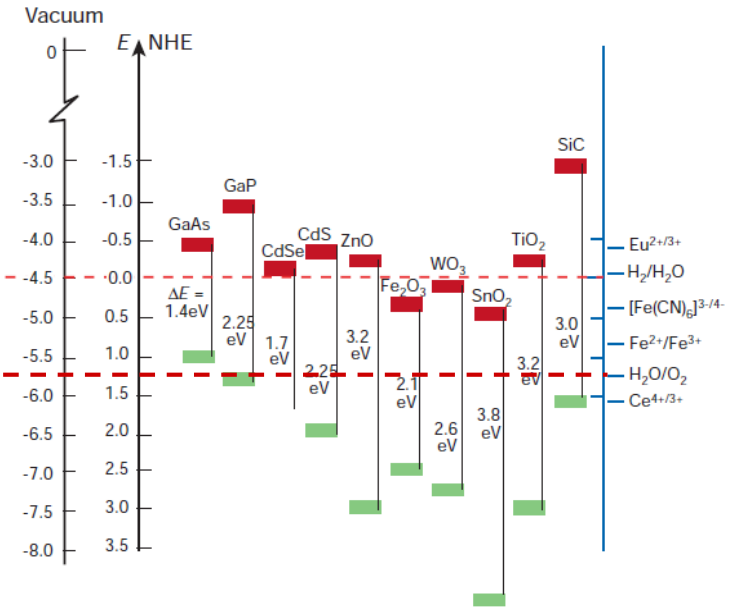

Figure 2-2 Band positions of common semiconductor materials in contact with aqueous electrolyte at *pH*=1. Two red dashed lines indicate hydrogen and oxygen evolution reaction potential. Several redox couple standard reduction potentials are also represented against NHE level.

Figure 2-2 lists band positions of common semiconductor materials in contact with aqueous electrolyte at *pH*=1 and the energy scale is indicated in eV using either normal hydrogen electrode(NHE) or vacuum level as reference.[5] Two red dashed lines represent the standard electrochemical evolution potential of H_2 and O_2 respectively. The overall photocatalytic reaction of water splitting can only take place when the energy of the absorbed photons is equal to or larger than the water splitting threshold energy of 1.23 eV which is calculated by equation 2.1 and 2.2, wherein ΔG^0 and ΔE^0 are Gibbs free energy change and standard electrochemical potential of the reaction under standard conditions, *n* is the number of charge involved in the reaction, and *F* is the Faraday constant. The mathematical representation below is referred to as the thermodynamic requirement for H_2 production by photoelectrolysis of water.

$$H_2O + h\upsilon \rightarrow H_2 + \frac{1}{2}O_2 \quad \text{.....2.1}$$

$$\Delta G^0 = -nF \cdot \Delta E^0 \quad \text{.....2.2}$$

In other words, the conduction band and valence band edges of the semiconductor material must straddle over the energy levels of H_2 and O_2 reduction potential simultaneously in order to split water. As seen in Figure 2-2, the conduction band edge of many semiconductors are more positive rather than negative position compared to the standard reduction potential of H_2, thus unable to produce H_2 through photoelectrolysis of water.

2.3.2 Kinetic Requirement

The above discussion addresses the thermodynamic requirement for photoelectrolysis of water by PEC. However, for meaningful water splitting efficiency, more important limitations that lie on reaction kinetics and thus requires significant overpotential as driving force must be overcome as oxygen evolution reaction at the cathode involves activation of multistep reactions. First, the semiconductor material must

be stable, corrosion-free, and non-reactive within selected electrolyte. Second and the most important, charge transfer after they are separated from the interface of semiconductor/liquid junction must be fast enough to prevent charge carrier recombination and energy loss be reduced due to overpotential.

2.4 Photoelectrochemical Solar Energy Storage

PECs can generate not only electrical but also electrochemical energy. Conversion of a regenerative PEC to a photoelectrochemical storage solar cell (PESC) can incorporate several increasingly sophisticated solar energy conversion and storage configurations.

Figure 2-3 presents an example of a PESC combining in situ electrochemical storage and solar-conversion capabilities, providing continuous output insensitive to daily variations in illumination. A high solar-to-electricity conversion efficiency (11.3%) was demonstrated using a PEC consisting of a Cd(Se,Te)/S_x and Sn/SnS storage system, resulting in a solar cell with a continuous output.[14] Under illumination, as seen in Figure 2-3(a), the photocurrent drives an external load. Simultaneously, a portion of the photocurrent is used to electrochemically reduce metal cations in the device storage half-cell. Under dark or below a certain level of illumination, the storage compartment spontaneously delivers power by metal oxidation, as seen in Figure 2-3(b).

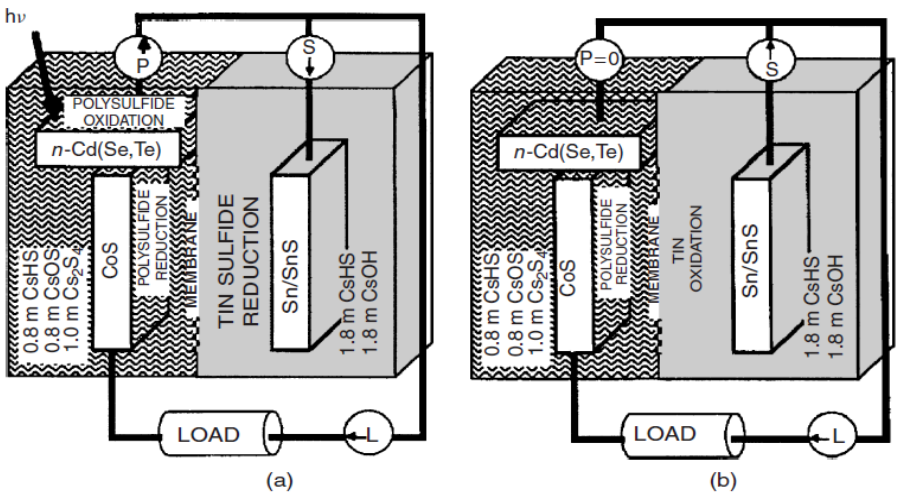

Figure 2-3 Schematic of a photoelectrochemical solar cell combining both solar conversion and storage capabilities. (a) Under illumination; (b) Under dark.

In light of such high solar-to-electrical (STE) conversion efficiency by realizing in-situ photoelectrochemical processes, a series of photoelectrochemical solar energy storage modes were either investigated or summarized by Stuart Licht.[15] Early studies on PESC systems have been performed on a variety of two-electrode configurations and important variations of these photoelectrochemical conversion and storage configurations are summarized in Table 2-1 and schematically shown in Figure 2-4.

In each case, exposure to light drives separate redox couples and a current through the external load. There is a net chemical change in the system, with an overall increase in free energy. In the absence of illumination, the generated chemical change drives a spontaneous discharge reaction. The electrochemical discharge induces a reverse current. In each case in Table 2-1, exposure to light drives separate redox couples and current through the external load. Consistent with Figure 2-1, in a regenerative PEC, illumination drives work through an external load without inducing a net change in the chemical composition of the system.

Table 2-1 List of exemplary photoelectrochemical conversion and storage modes using a two-electrode configuration.

SCHEME	*Electrode 1*	*Electrolyte(s)*	*Electrode 2*
I	SPE	| Redox A Redox B |	CE
II	SPE	| Redox A-membrane-Redox B |	CE
III	SPE	| Redox A |	Redox B_{CE}-CE
IV	SPE-Redox A_{SPE}	| Redox B |	CE
V	SPE	| Redox A-membrane-Redox B |	SPE

Note: Components of these systems include a semiconductor photoelectrode (SPE) and a counter electrode (CE). At the electrode–electrolyte interface, redox couples "A" or "B" are either in solution (| Redox |), counter electrode–confined (| Redox B_{CE}-CE) or confined to the semiconductor photoelectrode (SPE-Redox A_{SPE}|).

This compares with the two electrode PESC configurations shown in Figure 2-4. Unlike a regenerative system, there is a net chemical change in the system, with an overall increase in free energy. In the absence of illumination, the generated chemical change drives a spontaneous discharge reaction. The electrochemical discharge induces a reverse current. Utilizing two quasi-reversible chemical processes, changes taking place in the system during illumination can be reversed in the dark. Similar to a secondary battery, the system discharges producing an electric flow in the opposite direction and the system gradually returns to the same original chemical state.

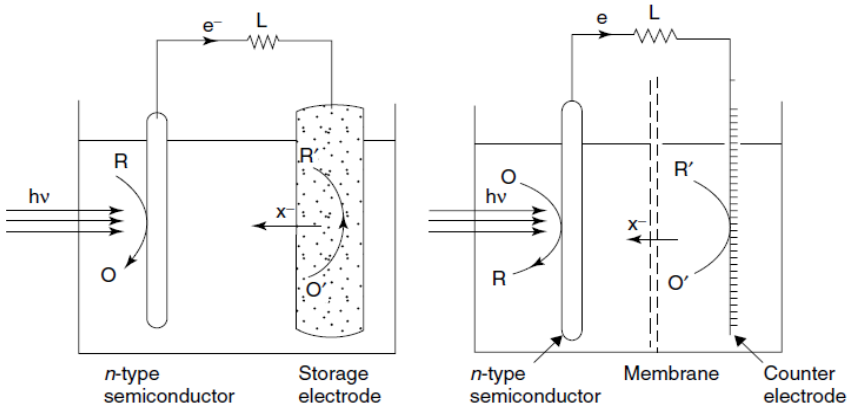

Figure 2-4 Cell structure of a PESC with (left) insoluble redox couple and (right) soluble redox couple.

However, both cells shown in Figure 2-4 have some disadvantages. Firstly, the redox species may chemically react with and impair the active materials of the photoelectrode. Furthermore, during the discharge process, the photoelectrode is kinetically unsuited to perform as an electrode for a reduction reaction in the absence of illumination. For the photoelectrode to perform efficiently during illumination (charging), such reduction process should be inhibited to minimize losses of back reaction which essentially cancel the photo-oxidation.

Hence, the same photoelectrode cannot efficiently fulfill the dual role of being kinetically sluggish to reduction upon illumination and yet being kinetically facile to the same reduction during discharge under dark. Meanwhile, the configuration represented in Figure 2-4 has another disadvantage, i.e., the disparity between the small surface area needed to minimize the losses due to the reverse reactions and the large surface area necessary to minimize storage polarization losses to maximize storage capacity.[16]

The above-mentioned disadvantages of using two-electrode configuration in PESC may be overcome by considering a third electrode (symbol A) in the cell as shown in Figure 2-5. In Figure 2-5, the switches E and F are generally alternated during charge and discharge. During the charging, only switch E may be closed, facilitating the storage process, and during discharge, E is kept open while F is closed. In this case, chemical changes that take place during the storage process are reversed, and a current flow is maintained from the storage electrode to a third (counter) electrode that is kept in the first compartment. To minimize polarization losses during the discharge, this third electrode should be kinetically active to the redox couple used in the first compartment.

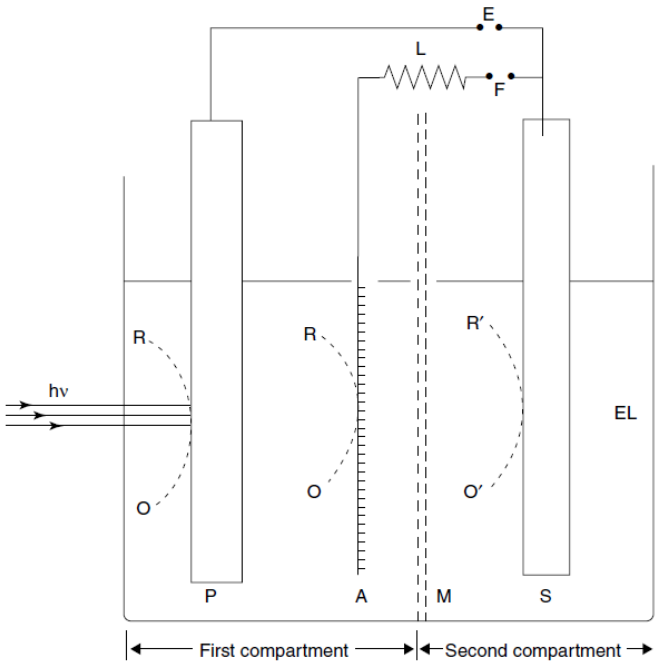

Figure 2-5 Cell structure of a PESC with a third electrode (counter electrode) in the photoelectrode compartment. P: Photoelectrode; A: Counter electrode; M: Membrane; S: Storage electrode; EL: Electrolyte; F: Electrical Switch and L: Load.

Still an improved situation would have both switches closed all the time. In this case, electric current flows from the photoelectrode to both the counter and storage electrodes. The system is energetically tuned such that when illumination is available, a significant fraction of the converted energy flows to the storage electrode. Under dark or diminished illumination, the storage electrode begins to discharge, driving continuous current through the load. In this system, a proper balance should be maintained between the potential of the solar energy-conversion process and the electrochemical potential of the storage process. There may be residual electric flow through the photoelectrode during dark cell discharge, as the photoelectrode is sluggish, but not entirely passive, to a

reduction process. This can be corrected by inserting a diode between the photoelectrode and the outer circuit.

2.4.1 Redox-assisted Solar Energy Conversion and Storage

Redox species, such as iodine, bromine, iron, cerium etc. in the electrolyte have been reported[17-21] to improve photocatalytic reaction rates for H_2 reduction/O_2 reduction half-cell reactions significantly and thus water splitting efficiency. These redox species serve as either electron donor or electron acceptor at the semiconductor/electrolyte interface to quickly scavenge charge carriers and enhance charge transfer due to their fast reaction kinetics.

Teruhisa Ohno and Michio Matsumura[20] discovered that photocatalytic oxidation of water on TiO_2 (rutile) powder proceeded with a fairly high efficiency (~9%) when iron (III) ions were used as the electron acceptor, which is in marked contrast to other reversible photocatalytic reactions, whose reaction rates decelerate as a result of the back reactions of the products on the photocatalysts. The efficient oxidation of water in the presence of iron (II) ions is attributed to preferential adsorption of iron (II) ions on TiO_2 over iron (III) ions, which enabled efficient oxidation of water.

The same group[17] also demonstrated a continuous water-splitting process into hydrogen and oxygen under photoirridation using two redox couples on suspended TiO_2 particles. In such a system, the reduction of water to hydrogen was realized by bromide ions, which were oxidized to bromine. On the other hand, oxygen was created through oxidation of water by Fe^{3+} ions, which were then reduced to Fe^{2+} ions.

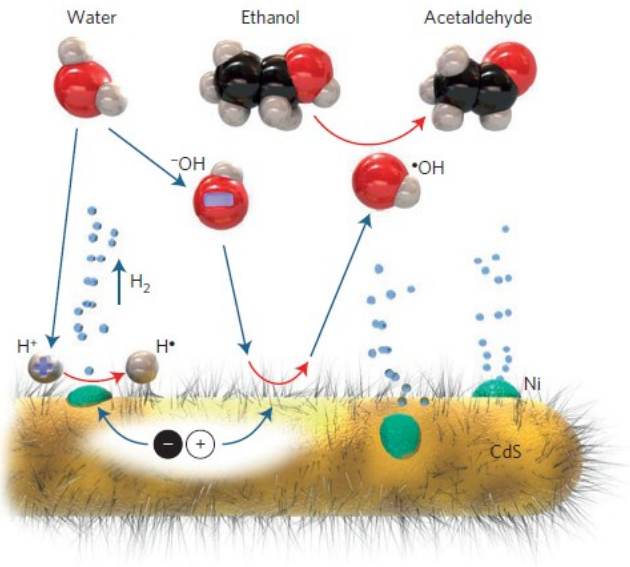

Figure 2-6 Schematic of the photocatalytic generation of H_2 under the proposed hole shuttle mechanism.

More recently, the collaboration[22] between a group of scientists from Germany and UK landed a remarkable increase in the H_2 generation rate on chalcogenide semiconductor nanocrystals by employing a $OH^-/OH^\bullet$ redox couple to efficiently relay the hole from the semiconductor to the scavenger.

The proposed two-step mechanism shown in Figure 2-6 of hole transfer employing a redox shuttle leads to a substantial improvement in the photocatalytic generation of hydrogen by the metal-semiconductor nanocomposites, up to 53% of external and 71% of internal quantum yield under 447 nm laser illumination, without the use of noble metal co-catalysts and protection against photo-oxidation of the photocatalyst. They concluded that the enhancement relies on much better mobility of the small molecular shuttle $OH^-/OH^\bullet$, and its efficient reactions with the semiconductor and the sacrificial agent, which implies that replacing the rate-limiting step with two faster

processes involving a redox mediator could be a viable approach to efficient photocatalysis.

2.5 Scope of Study and Objectives

In this study, we propose to use vanadium redox species (in the form of VO^{2+}/VO^{+} and V^{3+}/V^{2+}), the fundamental components of a vanadium redox battery(VRB) to convert and store solar energy due to the following unique characteristics:

i. Vanadium redox species and its behavior have been well studied back in 1980's and results lead to successful commercial products.

ii. Vanadium redox species have much faster kinetics in electrochemical reaction compared to H^{+}/H_2 and O_2/H_2O redox pairs in photocatalytic water splitting and therefore are prone to yield higher voltage and current efficiencies.

Our previous study demonstrated high reaction kinetics for VO^{2+}/VO^{2+} redox couples shown in Figure 2-7. The vanadium redox couple shows much higher current at the same overpotential. The exchange current density (i_0, marked by the arrows in Figure 2-7 lower graph) is calculated to be about six orders of magnitude higher than that of oxygen reduction reaction. Such a large i_0 would significantly compensate the overpotential (η) and thus improve solar energy conversion efficiency.

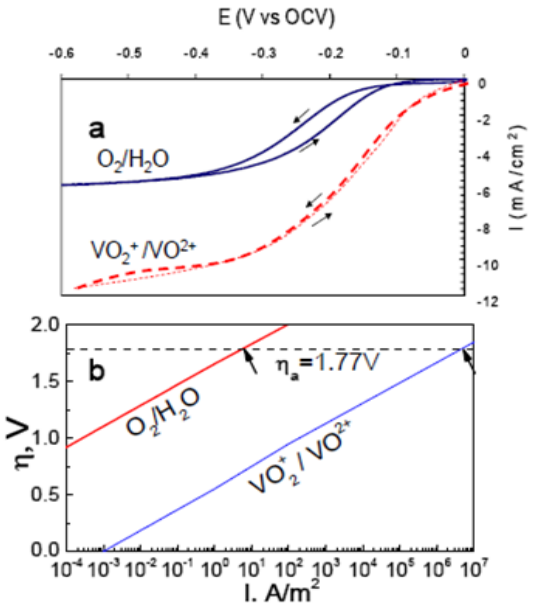

Figure 2-7 Kinetics comparison of reduction reaction of O_2/H_2O and VO^{2+}/VO^{+} in 3 M H_2SO_4.

iii. Simultaneous in-situ solar energy conversion and storage could be achieved. Figure 2-8 demonstrates such energy conversion approach, in a so-called all-vanadium photoelectrochemical cell as we developed in this dissertation.

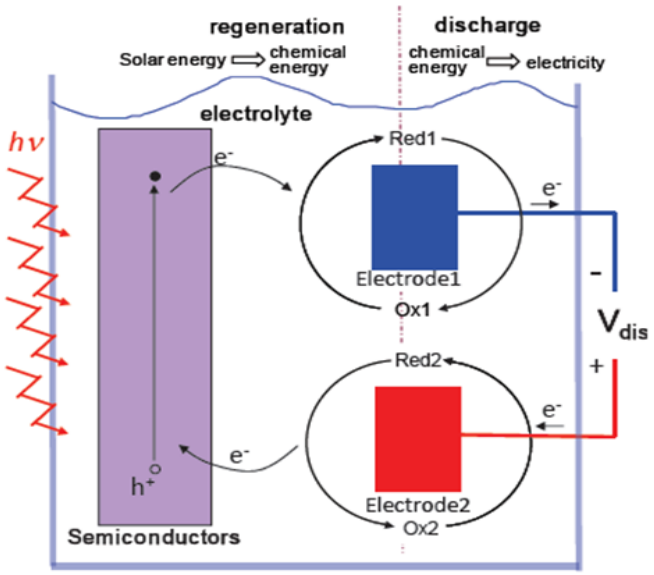

Figure 2-8 Schematic of the solar energy storage approach via photocatalytic redox reactions.

In such a PEC, a semiconductor material acts as photocatalyst/photoanode to convert and store solar energy into chemical energy by promoting oxidation/reduction reactions with two redox species, e.g., VO^{2+}/VO^{2+} and V^{3+}/V^{2+} in the electrolyte. During charge, the holes and electrons will oxidize and reduce different redox components at the anode and cathode, respectively, and thus achieve the goal of energy conversion. During discharge under dark, the energy stored in the redox species will be released by reversible electrochemical reactions if a load is connected.

Compared to conventional water splitting by a PEC, the proposed all-vanadium PEC excels in that the charge and discharge process can occur either separately or simultaneously, thus eliminating issues related to intermittent nature of solar illumination as a function of time or weather. Given the high reaction kinetics of vanadium redox species, a great enhancement on solar energy conversion efficiency would be expected if successful.

2.6 Description of This Dissertation

This dissertation is organized into the following chapters:

In Chapter 1, three major approaches to utilize solar energy are briefly introduced. The advantages and disadvantages of PECs, the most promising approach to generate either electricity or chemical fuel such as hydrogen, were elaborated and followed by the general description of the work demonstrated in this dissertation to conquer the major issues associated with conventional PECs.

In Chapter 2, fundamental aspects of PECs, including operating principles, thermodynamic and kinetic requirements in terms of photoelectrochemical water splitting will be presented. In addition, early work in the field with respect to photoelectrochemical solar energy storage will be summarized and the concept of redox-assisted solar energy conversion and storage will be disclosed. Finally, the scope and objectives of this study are proposed in details based upon our preliminary results.

In Chapter 3, photoelectrochemical studies have been performed on TiO_2 electrode and WO_3/TiO_2 hybrid electrode in an all-vanadium PEC to prove the concept of the proposed research. During the study, a photocharging/discharging process enabled by WO_3 acting as an effective electron storage reservoir was discovered.

In Chapter 4, the interaction between WO_3/TiO_2 hybrid electrode and vanadium redox reactions will be deeply investigated in an all-vanadium PEC using multiple electrochemical methods. A model aiming to explain the observed experimental results is proposed.

In Chapter 5, optimization of the photoelectrochemical performance of the all-vanadium PEC using a novel supporting electrolyte, methanesulfonic acid, has been performed in comparison with the system using sulfuric acid. The quantification that

defines the cell performance such as Faradaic efficiency and IPCE of the cell has been conducted.

In Chapter 6, all experimental results achieved from Chapter 3 to Chapter 5 in this dissertation are concluded.

Chapter 3

Primary Study of All-Vanadium PEC Using Different Photoelectrodes

3.1 Introduction

In this chapter, common photocatalysts, e.g., TiO_2 and WO_3, were employed to benchmark the photocatalytic properties of the proposed all-vanadium PEC. Not only we conducted the proof-of-the-concept experiments using a typical TiO_2 photocatalyst to test the system, but also an electron storage mechanism was discovered on WO_3/TiO_2 hybrid electrode preliminarily.

3.2 Experiments

3.2.1 Electrode and Electrolyte Preparation

Three types of photoelectrodes, TiO_2, WO_3, and WO_3/TiO_2 hybrid (12 wt% WO_3), were fabricated and used throughout the experiment. To fabricate the TiO_2 and hybrid electrodes, 0.997 g Degussa P25 TiO_2 (VP AEROPERL® by Evonik), 0.497 g ethyl cellulose (48.0-49.5%, Sigma-Aldrich USA), 0.124 g polyvindylidene fluoride (PVDF) powder (Kynar Flex 2801-00 by Arkema Group), 2.501 g α-terpineol (laboratory grade, Fisher Scientific USA) were mixed under constant stirring at 80°C for 1 h to obtain a uniform TiO_2 or hybrid slurry with the addition of 0.374 g tungstic acid (Alfa Aesar, USA) and 0.993 g hydrogen peroxide (35 %, Alfa Aesar USA). Then the slurry was deposited on a pre-cut square fluorine doped tin oxide (FTO) (sheet resistance 6-8 Ω/□, Pilkington USA) using a doctor blade. The FTO substrate was pre-washed with acetone (99.7%, Fisher Scientific USA), methanol (99.8%, Fisher Scientific USA), and deionized (DI) water, before being blow-dried and then further dried in an oven at 120°C for 1h. After the deposition, the obtained coating was dried in the oven for 1 h and then calcined under air flow at 325°C for 5 min, 375°C for 5 min, 450°C for 15 min, and finally 500°C for 15 min.

The fabrication of WO_3 electrode was performed in a similar manner. After the fabrication, the active electrode area was approximately 6.45 cm^2.

Four types of electrolytes, 3 M H_2SO_4, 0.1 M vanadium(IV, VO^{2+}) in 3 M H_2SO_4, 0.01 M vanadium(IV) in 3 M H_2SO_4,and 0.01 M vanadium(III, V^{3+}) in 3 M H_2SO_4, were used in the experiments. The first three electrolytes were prepared by dissolving stoichiometric amount of H_2SO_4 (96.6%, J.T. Baker USA) in DI water with or without vanadium(IV) sulfate oxide hydrate ($VOSO_4 \cdot xH_2O$) (99.9%, Alfa Aesar USA). The number of hydrate in $VOSO_4 \cdot xH_2O$ was pre-determined by thermogravimetric analysis. The prepared 0.01 M vanadium(IV)-sulfuric acid and 0.1 M vanadium(IV)-sulfuric acid electrolytes appear light blue and blue respectively. The 0.01 M vanadium(III) electrolyte was obtained by electrochemically reducing the prepared vanadium(IV)-H_2SO_4 solution in an electrochemical cell at a constant current density of 3 mA/cm^2 using a potentiostat (Princeton Applied Research, PARSTAT 2273) until the potential reached 1.6 V. During the reduction, the electrolyte was protected by N_2 throughout the experiment to prevent oxidation of vanadium(III) species. The obtained 0.01 M vanadium (III)-sulfuric acid solution appeared light green.

3.2.2 Cell Design and Assembly

Linear sweep voltammetry (LSV), cyclic voltammetry (CV), and zero-resistance ammetry (ZRA) were conducted in either a half-cell configuration(one chamber) or full-cell configuration (two chambers filled with VO^{2+} and V^{3+}electrolytes, separated by a Nafion117 membrane) with their schematics shown in Figure 3-1. In both cell configurations, the photoelectrode serves as the working electrode (WE) while a platinum mesh and Ag/AgCl electrode serve as the counter electrode (CE) and reference electrodes (RE), respectively. The voltage scan ranged from -0.197 to 1.3 V with 0.1 V interval of dark/illumination. The overall duration for ZRA measurement was180 s with 20

s intervals of dark/illumination. The solar irradiation was created using an ozone-free solar simulator system (Newport USA) coupled with an AM 1.5 global filter (Newport USA) and calibrated using a standard Si photodiode (Newport USA).

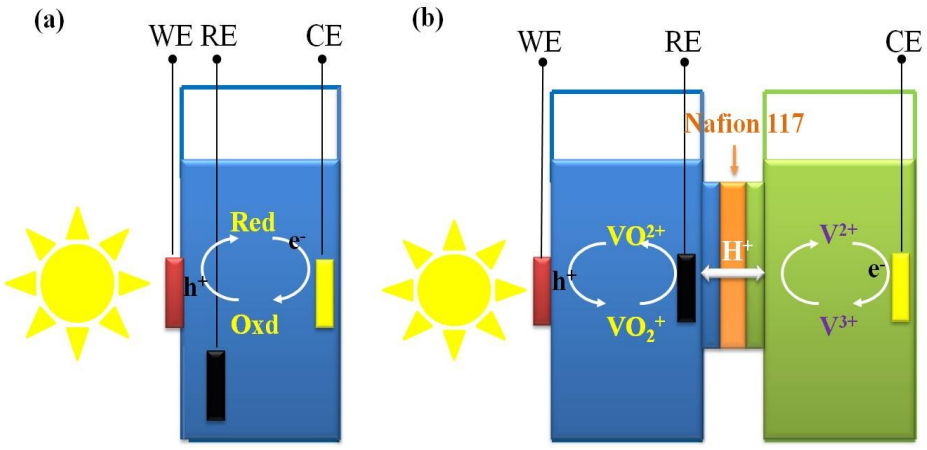

Figure 3-1 The representative schematics of (a) half-cell configuration and (b) full-cell configuration.

3.2.3 Material Characterization

The crystallographic information of the electrodes was determined by XRD (Siemens, 810-M340-32-C3000) at a scan rate 0.01° s^{-1} between 20°-80° with a dwell time of 1 s. Scanning electron microscopy (Hitachi S-3000N variable pressure SEM) was used to examine the microstructure of photoelectrodes. The energy dispersive spectroscopy (EDS) mapping was also performed to reveal elemental composition of the sample. The UV-Vis diffuse reflectance spectra of the samples were obtained on a JASCO V-570 spectrophotometer while Raman spectra were collected on a PerkinElmer DXR Raman microscope.

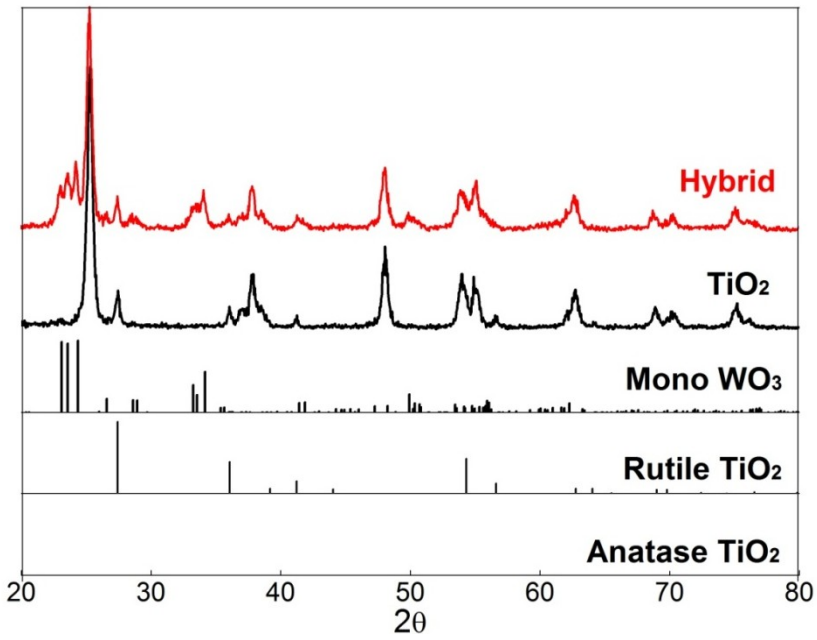

Figure 3-2 XRD spectra of the TiO_2 and WO_3/TiO_2 (12 wt% WO_3) hybrid electrodes.

Figure 3-2 presents the XRD spectra of the TiO_2 and WO_3/TiO_2 (12 wt% WO_3) hybrid electrodes. The JCPDS standards for anatase TiO_2 (#21-1272), rutile TiO_2 (#76-1940), and monoclinic WO_3 (#83-0950) were also shown as reference. It is found that only anatase and rutile phases of TiO_2 existed in both samples with the former being predominant. This finding is in agreement with the revealed phase information of the commercial Degussa P25 product. Also, only monoclinic phase of WO_3 was found in the hybrid sample, and no noticeable impurity phase such as bromite TiO_2 or orthorhombic or tetragonal WO_3 existed by cross-referencing the XRD spectra with the standards.

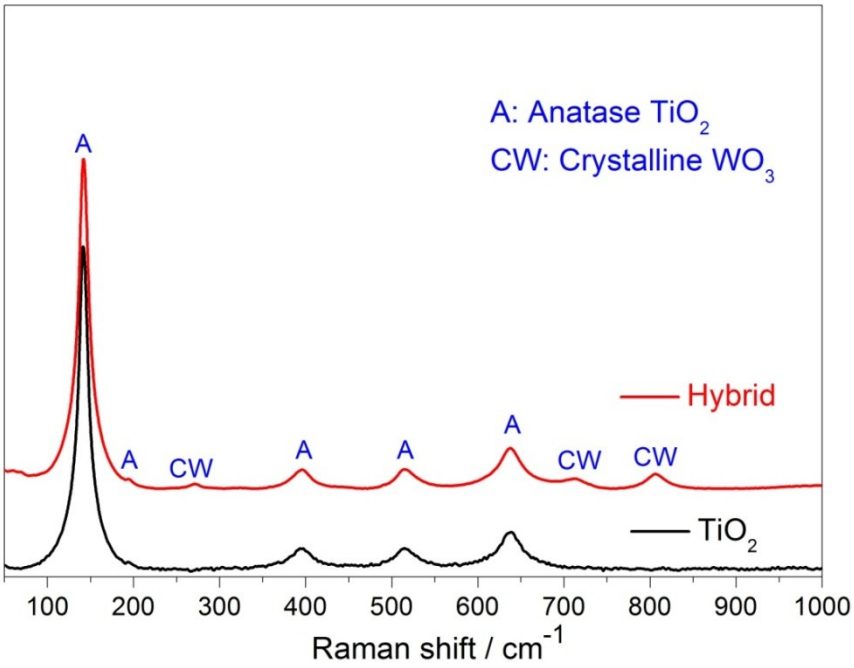

Figure 3-3 Raman spectra of the TiO_2 and WO_3/TiO_2 (12 wt% WO_3) hybrid electrodes.

Raman spectroscopy was employed to verify the phases of TiO_2 and WO_3 along with carbon species in the photoelectrode. In Figure 3-3, five Raman active modes near 146, 197, 397, 515, and 633 cm^{-1} are clearly observed for both samples. These peaks are characteristic vibration modes of a TiO_2 anatase phase. No TiO_2 rutile phase is observed even though it was reported to appear near 455 cm^{-1}.[23] The vibration modes of graphitic carbon (1200-1600 cm^{-1}) were not observed (results not shown), which indicates that carbon species were all removed during the sintering process. The band near 270 cm^{-1} is emerging from the O-W-O deformation vibration and bands around 713 and 806 cm^{-1} are attributed to the O-W-O stretching vibrations.[23, 24] All these bands belong to the characteristic vibration modes of monoclinic WO_3 and all Raman results are consistent with XRD patterns revealed in Figure 3-2.

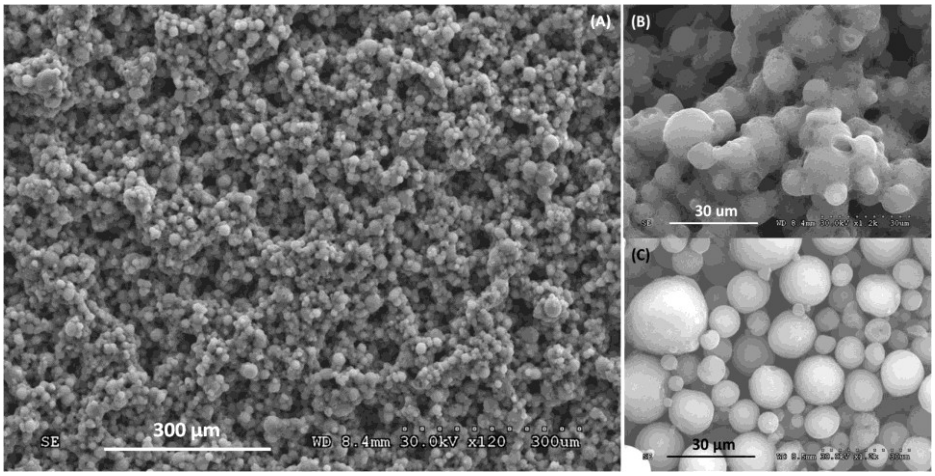

Figure 3-4 SEM images of sintered TiO_2 sample in (A) lower and (B) higher magnification, together with (C) unsintered TiO_2 powder.

Figure 3-4 demonstrates morphologies of the sintered TiO_2 photoelectrode in comparison with the unsintered TiO_2 powder. It is seen from Figure 3-4A that a continuous porous network of TiO_2 is formed by randomly-organized spherical particles ranging from 3-25 µm and no explicit crack was found in the sample. A close view of the particles shown in Figure 3-4B reveals that the sintered TiO_2 sample has its particles adjoined together due to heat treatment and craters/irregularities of various sizes are found to exist on the surface rendering it very rough. On the contrary, the unsintered TiO_2 powders (Figure 3-4C) were composed of many isolated spheres with relatively smooth surface although particle size remains unchanged.

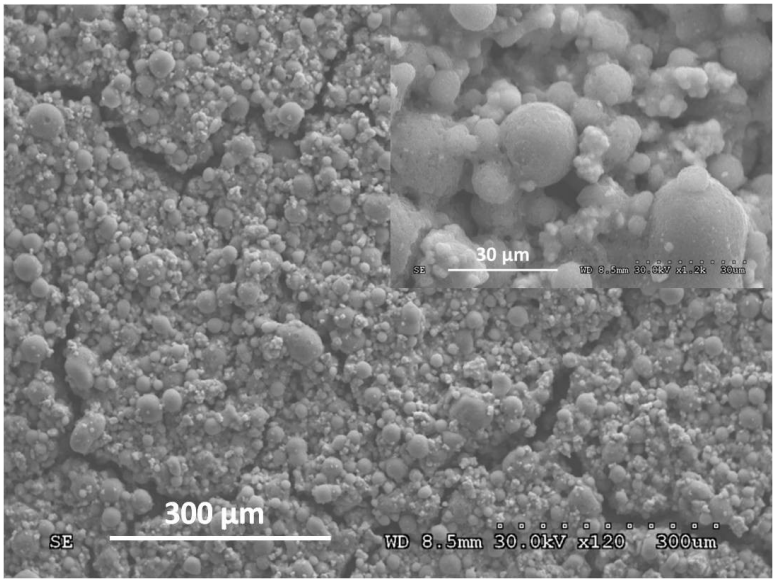

Figure 3-5 SEM image of the WO_3/TiO_2 (12 wt% WO_3) hybrid electrodes. A higher-magnification image is shown in the inset.

SEM images were also taken on the hybrid electrode in Figure 3-5 in order to compare with the pure TiO_2 electrode. Possessing a similar porous network to the pure TiO_2 electrode as demonstrated in Figure 3-4A, the hybrid sample, however, exhibites a binomial distribution of particles consisting mainly of large TiO_2 particles along with small WO_3 particles of 1-2 μm that are embedded discretely in the matrix. TiO_2 particles are adjoined with not only themselves but also their neighboring WO_3 particles. Many mini-cracks are found to exist in the matrix. As seen in the inset image, WO_3 particles tend to agglomerate more easily than TiO_2 due to their much smaller dimensions and they were also found to be scattered on the surface of TiO_2 particles. Note that the size of TiO_2 particles in the hybrid sample remains unchanged compared to that of the pure TiO_2 sample.

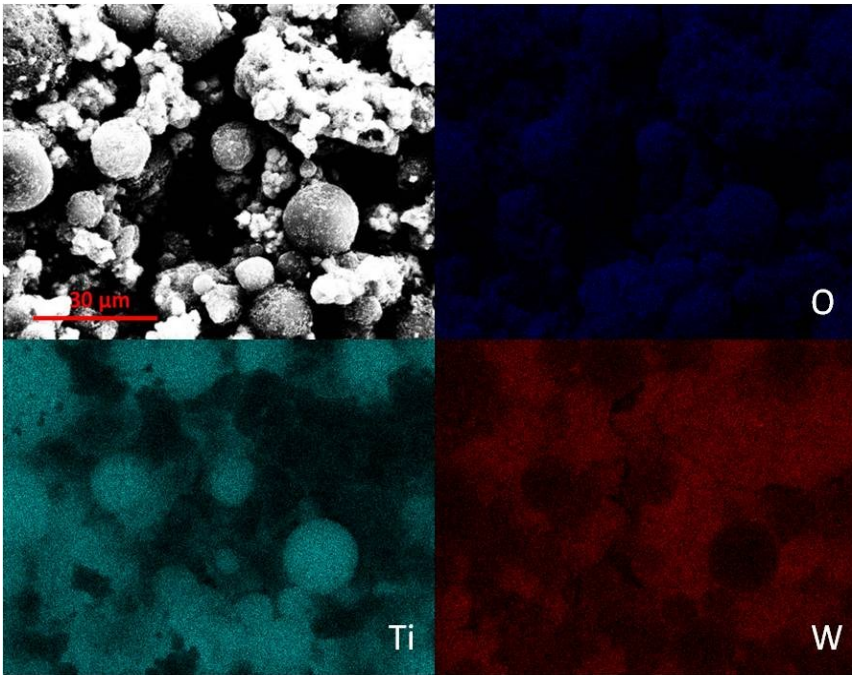

Figure 3-6 EDS mapping result of the WO_3/TiO_2 (12 wt% WO_3) hybrid electrode.

WO_3 particles were found to distribute all over the matrix in the hybrid electrode, according to EDS mapping result shown in Figure 3-6. Only three elements, Ti, W, and O were found to exist in the sample analyzed by EDS and TiO_2 was demonstrated to dominate in the electrode over WO_3 as indicated by rather distinguished Ti element on the mapping graph. On the other hand, WO_3 particles were also found to scatter around and over the TiO_2 particles and such intimate contact between the two semiconductors is expected to facilitate charge carrier transfer between WO_3 and TiO_2, and reduce their recombination after they are generated.

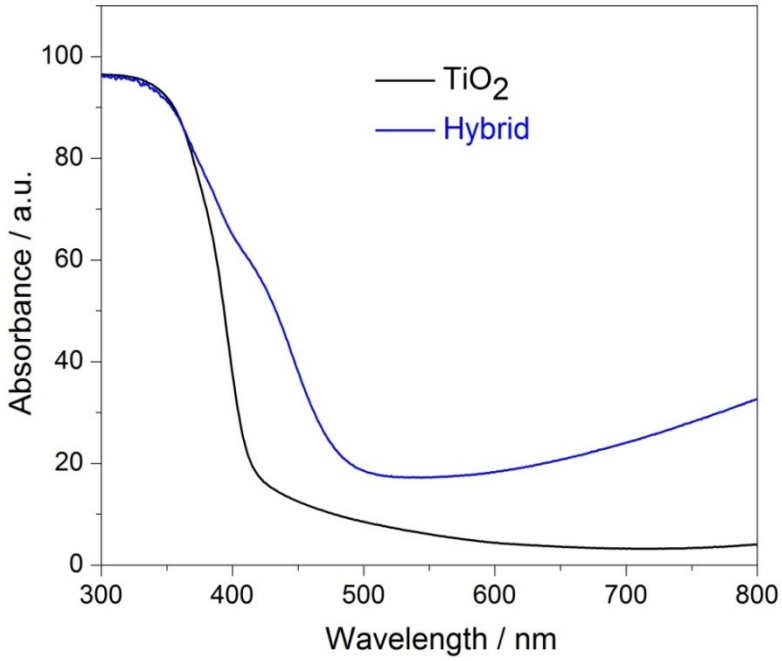

Figure 3-7 UV-Vis diffuse reflectance spectra of the TiO_2 and WO_3/TiO_2 (12 wt% WO_3) hybrid electrodes.

The optical property of both the TiO_2 and hybrid electrodes was studied by UV-Vis diffuse reflectance spectroscopy and the spectra are revealed in Figure 3-7. For TiO_2, the absorption edge resides in near 380 nm as TiO_2 is well known to absorb only the UV light. The hybrid sample shows a clear red shift on the spectrum, extending the absorption edge into the visible light region near 450 nm. Compared to the pure TiO_2 sample, the hybrid one also demonstrates an improved absorption tail ranging from 500 to 800 nm, which is ascribed to the smaller band energy of 2.6-2.8 eV of WO_3.[24-26]

3.3 Photoelectrochemical Study

3.3.1 Proof-of-the-concept Experiment

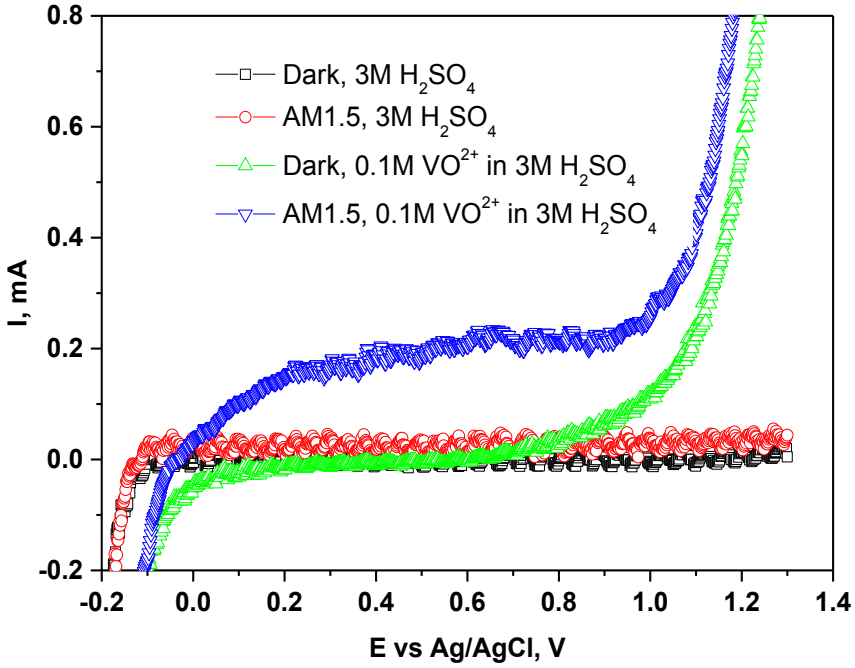

Figure 3-8 The linear sweep voltammograms of the TiO_2 electrode under various electrochemical conditions in a half-cell configuration. The scan rate was 5 mV/s.

The proof-of-the-concept experiment was conducted using the TiO_2 electrode by LSV under various electrochemical conditions in a half-cell configuration. The results shown in Figure 3-8 clearly indicate that vanadium redox species (VO^{2+} in this experiment) is capable of improving photocatalytic property of PEC significantly, in other words, the feasibility of our hypothesis.

As seen in Figure 3-8, little difference in photoelectrochemical response of the TiO_2 photoelectrode is observed regardless of the presence of illumination when only acid was employed as the electrolyte. Furthermore, the barely noticeable photocurrent throughout the potential window under illumination manifests the well-known wide

bandgap of TiO_2[7] and its notorious electron-hole pair recombination at the semiconductor/liquid junction interface. However, the addition of VO^{2+} species in the electrolyte abruptly changes the voltammetry response as depicted in Figure 3-8, especially under illumination. Two distinct photoelectrochemical behaviors are seen when VO^{2+} species participate the electrochemical and/or photoelectrochemical reactions. At potentials less positive than 1.0 V, TiO_2 shows a typical n-type semiconductor photoelectrochemical behavior in 0.1 M-3 M H_2SO_4 electrolyte under AM 1.5 illumination, except that the photocurrent achieved is magnificently enhanced on average 14 times higher than that with only 3 M H_2SO_4 as the electrolyte from 0.0 to 1.0 V. The significant improvement in photoresponse is believed to be induced by a synergistic effect of photocatalysis of TiO_2 and oxidation of VO^{2+} species. Fast electrochemical kinetics of VO^{2+} oxidation (at least six orders of magnitude higher than the oxygen evolution) is believed to quickly scavenge holes. This thus minimizes charge recombination and improves photocatalytic electron-transfer efficiency at the semiconductor interface.[9] The other interesting electrochemical and/or photoelectrochemical behavior of TiO_2 in 0.1 M V-3 M H_2SO_4 electrolyte appears at potentials more positive than 1.0 V. The current increases abruptly as the potential increases regardless of the illumination, which may be ascribed to tunneling effect of electrons across the semiconductor/liquid junction in both dark and illumination conditions.

In classic photoelectrochemistry of semiconductors,[5, 6, 8-10, 27-29] when light illuminates upon a n-type semiconductor immersed in a liquid solution containing a redox species, oxidative electron transfer reaction occurs at the semiconductor interface once the electrolyte redox potential is positioned below that of the photogenerated hole at edge of the bended valence band of the semiconductor. As a result, the redox species will be oxidized photo-electrochemically. In our study, as the potential scale for the upper edge

of valence band of TiO_2 against NHE (Normal Hydrogen Electrode) in contact with aqueous solution at *pH*=1 is approximately 2.8 V[5] and the standard potential of V^{4+}/V^{5+} redox is 1 V,[30] it is obviously facile for the VO^{2+} species to be quickly oxidized by scavenging the holes at the semiconductor surface according to the principle mentioned above, which consequently reduces the electron-hole pair recombination and enhances the photoresponse. Note that the instability of voltammetry signals between 0.2 to 0.8 V is believed to be caused by the possible competing scavenging process of photogenerated holes among a series of vanadium species complex[31-33] though V(IV) species exists predominantly in the form of VO^{2+} in *pH*<1 acidic solution.[34]

The effect of vanadium species concentration on the current under both dark and illumination conditions was also studied and the results are shown in Figure 3-9. Two photocurrent ratios at both 0.5 and 1.0 V, including those between oxidation of VO^{2+} (V) and water (W) (Figure 3-9A) and between those under illumination and dark (Figure 3-9B) for vanadium species, are shown. Figure 3-9A clearly shows that at a lower potential (0.5 V) the photocurrent ratio between oxidation of VO^{2+} (V) and water (W)slightly increases with increasing VO^{2+} concentration (below 0.5 M). However, the ratio becomes saturated and even reduces when the VO^{2+}concentration is beyond 0.5 M, which is suspected to be caused by incorporation of vanadium species into TiO_2 lattice and therefore deactivation of the semiconductor. At a higher potential (1.0 V vs. Ag/AgCl), the ratio improves significantly suggesting fast photoelectrochemical kinetics of the VO^{2+} species. On the other hand, the photocurrent ratio between those under AM 1.5 and dark shown in Figure 3-9B decreases with VO^{2+} concentration, suggesting that at higher concentrations the oxidation current from purely electrochemical reaction may dominate over the photoelectrochemical process. The above-mentioned results indicate that the proposed vanadium ions are very photo/electrochemically active. To effectively reveal the

photoelectrochemical storage/conversion using these redox species, lower concentration and lower voltage (particularly, no external bias) are preferred.

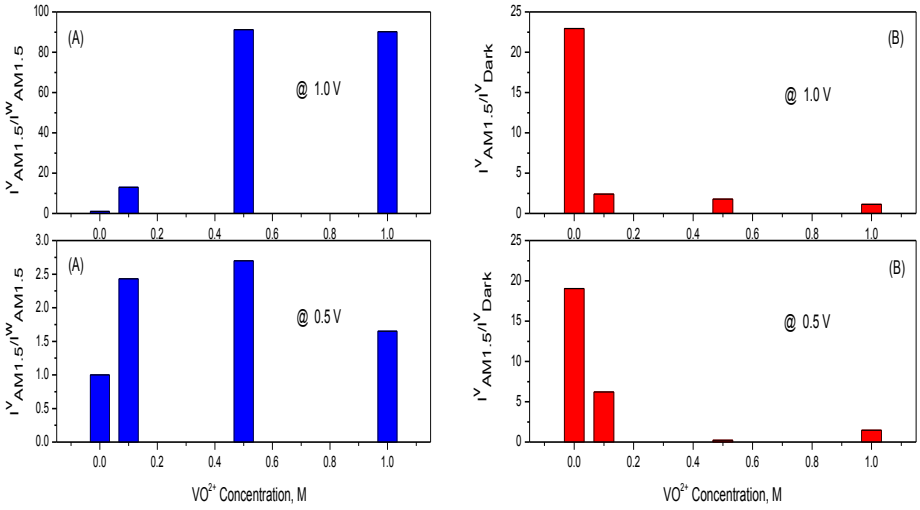

Figure 3-9 The plot of (a) $I^{V}_{AM1.5}/I^{W}_{AM1.5}$ and (b) $I^{V}_{AM1.5}/I^{V}_{Dark}$ as a function of vanadium species concentration at 0.5 V and 1V.

3.3.2 Photoelectrochemical Performance of the Hybrid Electrode

The above results have clearly demonstrated significant ability of vanadium redox species in enhancing photoelectrochemical performance of the PEC and thereof the feasibility of the proposed hypothesis. To further improve the photocatalytic property of the PEC, we also fabricated WO_3/TiO_2 hybrid electrode (12 wt% WO_3) and compared its photocatalytic performance with TiO_2 electrode under various electrochemical circumstances.

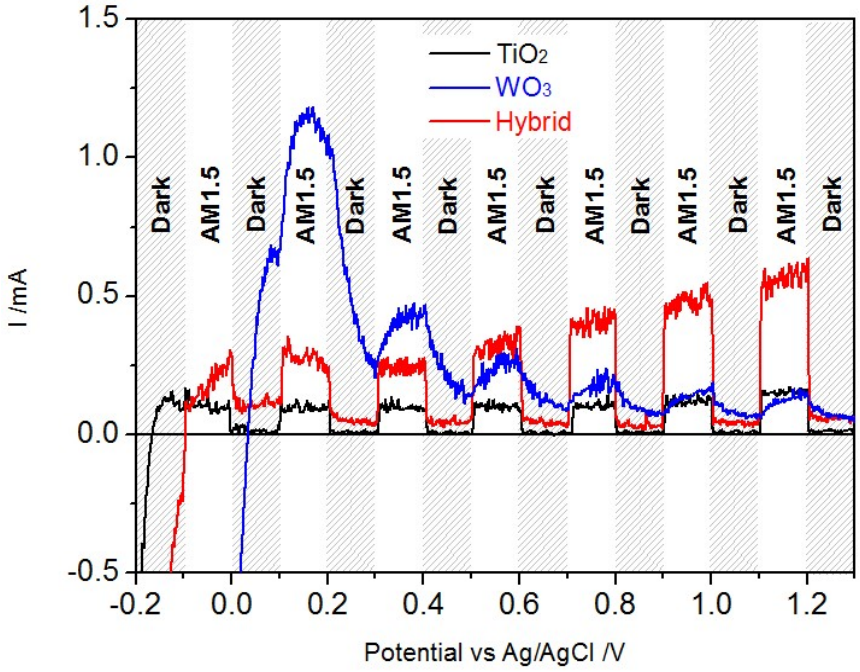

Figure 3-10 Linear sweep voltammograms of three different electrodes in 3 M H_2SO_4 electrolyte in a half-cell configuration under alternate dark and illumination conditions. The scan rate was 5 mV/s.

To compare the photoelectrochemical performance of different electrodes, LSV was firstly employed in a half-cell configuration in the experiment and the results are shown in Figure 3-10. The results show insignificant photocurrents of TiO_2 and WO_3 electrodes under AM 1.5 illumination. However, the hybrid electrode exhibited much more noticeable photoelectrochemical response corresponding to a higher reaction rate of the following equation particularly at

higher potentials.

$$VO^{2+} + H_2O \rightarrow VO^{+} + e^{-} + 2H^{+} \quad (E_0=1.0\ V) \text{.....3.1}$$

Besides, the photocurrent of TiO_2 and WO_3 electrodes remained almost unchanged at higher potentials under illumination whereas the photocurrent of the hybrid

electrode was enhanced at least by a factor of 3-4. The enhanced photoresponse is clearly indicative of mitigated charge recombination and thus improved photoelectrochemical reaction rate. It was well reported in literatures[24-26, 35] that monoclinic WO_3 has a more positive valence band (VB) than TiO_2 and photogenerated holes tend to migrate from its VB to that of TiO_2 and then to the catalyst surface under illumination. Electrons, however, favor migrating from the conduction band (CB) of TiO_2 to that of WO_3 and then to the bulk of the semiconductor due to the more negative potential of TiO_2 CB. As a result, the photogenerated charge carriers would tend to separate rather than recombine in the bulk, leading to a significant improvement in photocurrent. What's also worth mentioning in Figure 3-10 is that a broad peak emerges around 0.1 V on the anodic scan. This is believed due to *electrochromism/photochromism* of WO_3 under certain electrochemical conditions and the detailed study of this observation is given later.

As evidenced in our previous work,[36] fast redox reactions using vanadium redox couples are capable of boosting photoelectrochemical performance via quickly scavenging holes at the semiconductor/electrolyte interface and thus mitigating recombination of charge carriers after they are generated. However, our previous study of such effect relied on cyclic voltammetry that requires an external bias applied to the cell. In the study performed herein, zero-resistance ammetry (ZRA) method was adopted in the experiments to investigate the photoelectrochemical properties of different electrodes and the results are given in Figure 3-11.

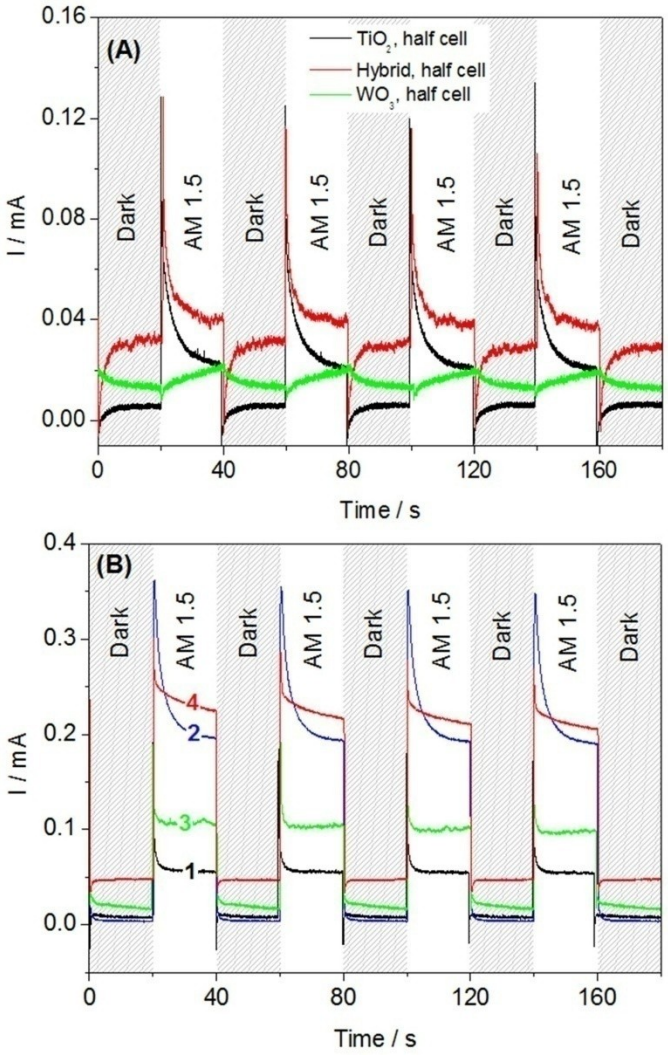

Figure 3-11 Photocurrents of different photoelectrodes using ZRA method in (A) 3 M H_2SO_4 electrolyte and (B) various vanadium electrolytes in different cell configurations. The labels in Figure 3-11B designate: 1: TiO_2 in 0.01 M V(IV)-H_2SO_4, half-cell; 2: TiO_2 in 0.01 M V-H_2SO_4, full-cell; 3: Hybrid in 0.01 M V(IV)-H_2SO_4, half-cell; and 4: Hybrid in 0.01 M V-H_2SO_4, full-cell.

Figure 3-11A compares the photoresponse of three different photoelectrodes in 3 M H_2SO_4 electrolyte with a half-cell configuration while Figure 3-11B compares TiO_2 and

hybrid electrodes with a full-cell configuration. As revealed in both graphs, the hybrid electrode shows a more pronounced photocurrent than TiO_2 or WO_3 electrode regardless of the electrolyte and cell configuration. Such improvement is ascribed to facilitated charge carrier transfer from WO_3 to TiO_2 due to their band structure interplay, as discussed earlier.

On the other hand, the vanadium redox pairs have a great contribution toward photocurrent enhancement regardless of the electrode used. This enhancement is even more conspicuous when two vanadium redox species, i.e., VO^{2+} and V^{3+}, and a full-cell configuration were coupled with each other. As indicated by the black and red curves in Figure 3-11A, the photoelectrochemical performance of both TiO_2 and hybrid electrodes in 3 M H_2SO_4 was unsatisfactory in terms of photocurrent magnitude. However, the addition of vanadium redox species even with a small molarity of 0.01 M (black and green curves in Figure 3-11B) at least doubled the photocurrent for both electrodes, which again proves the fast reaction kinetics of vanadium redox pairs.

Furthermore, when two pairs of vanadium redox species were used in separate chambers with a full-cell configuration, the photocurrent was significantly boosted for both electrodes especially the hybrid one, as clearly demonstrated by the blue and red curves in Figure 3-11B. Instead of the hydrogen evolution reaction taking place with a half-cell configuration, reduction reaction of the following equation occurred at the counter electrode in a full-cell configuration, which is responsible for the improved photocurrent.

$$V^{3+} + e^- \rightarrow V^{2+} \qquad (E_0\text{=-0.26 V}) \text{.....} 3.2$$

3.3.3 Preliminary Electron Storage Study by Hybrid Electrode

It is also interesting to note in Figure 3-11 that the hybrid electrode showed a noticeable dark current after the illumination was switched off, which indicates its greater ability to store electrons and release of the stored electrons. We ascribe this occurrence

to the formation of tungsten bronze induced by the photocharge/discharge process under higher energy irradiation on the WO_3 surface. It is known that WO_3 tends to be electrochemically reduced to tungsten bronze by combining electrons and protons (H^+) under UV irradiation as depicted in the following equation: [37-39]

$$WO_3 + xe^- + xH^+ \underset{\text{discharge}}{\overset{\text{photocharge}}{\longleftrightarrow}} H_xWO_3 \quad \text{.....3.3}$$

Due to such reaction, the surface of the photocatalysts, *i.e.,* TiO_2 and WO_3, will be covered with H_xWO_3, which prevents the photogenerated holes from moving from the valence band of WO_3 to that of TiO_2 and further to semiconductor/liquid interface to oxidize VO^{2+} ions. This thus compromises photocatalysis of the semiconductor materials. When irradiation was turned off, tungsten bronze undergoes discharge/self-discharge, which transforms itself back to WO_3. As a result, more semiconductor material will rejoin the photocatalysis process. Furthermore, the transfer of the photogenerated holes may be again possible from the WO_3 valence band to the TiO_2 valence band, thus enhancing the photocurrent. This photocharge/discharge process was confirmed by the blue appearance of the electrode under AM 1.5 irradiation and disappearance under dark through certain period of time. However, different from the electrode's behavior in Figure 3-11A, charge carriers can be quickly consumed by the vanadium redox species in the electrolyte especially in a full-cell configuration and thus renders a negligible dark current.

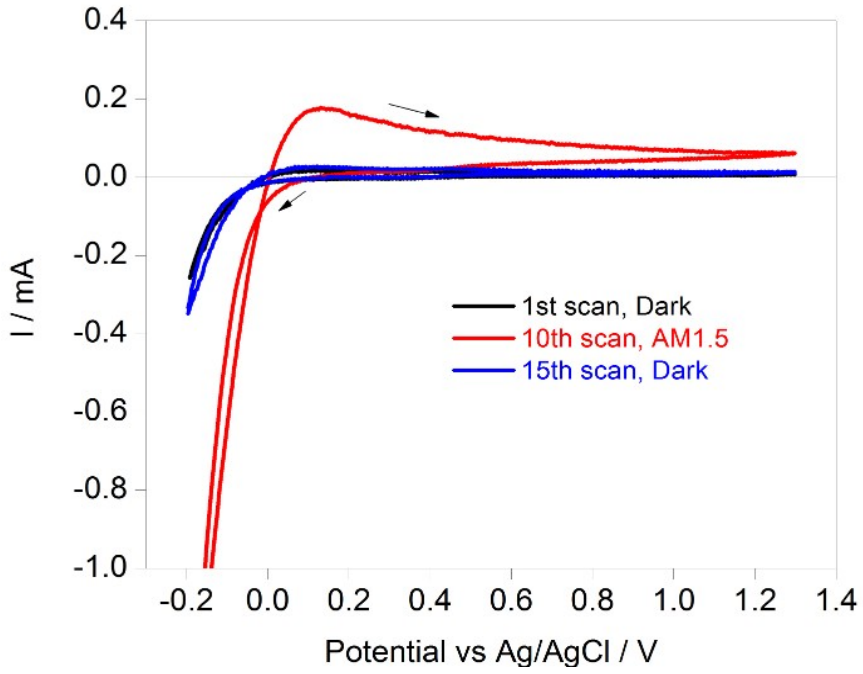

Figure 3-12 CV of the WO_3 electrode in 3 M H_2SO_4 electrolyte under dark and AM 1.5 illumination in a half-cell configuration. The scan rate was 20 mV/s.

It has been reported[26, 40-42] that storage of photogenerated electrons in WO_3 is achievable under one or more of the following conditions: (i) the presence of UV illumination and a hole scavenger, (ii) application of a negative bias, and/or (iii) use of an external source of electrons. To further study the formation of tungsten bronze, multiple CV scans were conducted on the pure WO_3 electrode in 3 M H_2SO_4 electrolyte under alternate dark/illumination to eliminate the effect of other factors, such as hole scavengers and external electrons provided by TiO_2 for instance. The first nine cycles were conducted under dark and all CV curves overlapped with each other as shown in Figure 3-12. This result indicates that no detectable electrochemical reactions occurred on the electrode in an acidic environment under dark conditions. At the 10^{th} scan, when AM 1.5 illumination was applied, the WO_3 electrode showed a broad peak centered

around 0.1 V due to the formation of tungsten bronze from WO_3 reacting with H^+ ions and the photogenerated electrons.[36, 40, 42] The anodic current induced by the illumination is appreciable throughout the potential window and the cathodic current at potentials below 0.05 V vs. Ag/AgCl results from the decomposition of tungsten bronze that releases both H^+ ions and electrons. These peaks disappeared when AM 1.5 illumination was turned off at the 11^{th} scan and the current went back to the original value eventually at the 15^{th} scan, indicating a reversible behavior of the reactions.

The integration of a WO_3/TiO_2 hybrid electrode and vanadium redox pairs offers a new approach to efficiently store solar energy. The vanadium redox pairs serve two purposes: (i) quickly scavenge the charge carriers, mitigate their recombination and thus boost the photocurrent, and (ii) shift the dynamic equilibrium between charge carrier recombination and redox reaction toward the latter due to fast kinetics of these vanadium redox couples. The hybrid electrode is able to not only effectively facilitate charge transfer between the two semiconductors and enhance the light absorption, but also serves as electron storage reservoir. The latter is critical to yield constant PEC reactions that are responsible for the regenerative solar energy storage. The built-in electron reservoir in the photoelectrode would result in stable electron storage and supply albeit the intermittent nature of sunlight.

3.4 Conclusion

Three types of photoelectrodes, TiO_2, WO_3, and WO_3/TiO_2 hybrid electrode (12 wt% WO_3) were fabricated and their photoresponse was investigated by CV and ZRA under various electrochemical and photoelectrochemical conditions.

The proof-of-the-concept experiment was conducted using LSV in 0.1 M V-H_2SO_4 electrolyte under AM 1.5 illumination and the results clearly reveal a significant photoresponse enhancement compared to photolysis of water even with a pristine TiO_2

electrode. This is attributed to the hole scavenging process initiated by quick redox reaction and depressed charge recombination at semiconductor/liquid interface.

In order to further improve photoelectrochemical performance of the PEC, a WO_3/TiO_2 hybrid electrode (12 wt% WO_3) was fabricated and probed using CV and ZRA. The hybrid electrode exhibited higher photoresponse than TiO_2 electrode and this improvement is ascribed to facilitated charge carrier transfer from WO_3 to TiO_2 due to their band structure interplay.

Meanwhile, an all-vanadium photoelectrochemical storage cell has been demonstrated by coupling two vanadium redox pairs instead of one with either TiO_2 or WO_3/TiO_2 hybrid electrode. The photoelectrochemical study performed shows the photocurrent has been significantly enhanced with the assistance of two vanadium redox pairs especially using a TiO_2/WO_3 hybrid electrode. It is believed that the vanadium redox pairs play a key role in the regenerative solar energy storage due to their fast reaction kinetics.

Various material characterization was also conducted on all used electrodes and the results imply that an intimate contact between WO_3 and TiO_2 is key to enhancement in charge carrier transfer, depression of recombination, and improvement in the photocurrent.

Most important, a photocharge/discharge process was discovered on the WO_3 under different energy level of irradiation, leading to a deteriorated photocurrent. This interesting phenomenon is found to be associated with the formation/decomposition of tungsten bronze under higher or lower energy of irradiation respectively. The preliminary study of hybrid electrode in combination with vanadium redox reactions demonstrates that WO_3 therein functions as an effective electron storage reservoir, which would

potentially enable a unique dual solar/electron storage system albeit the intermittent nature of sunlight.

Chapter 4

Electron Storage Study of Hybrid Electrode

4.1. Introduction

In chapter 3, we proved the great ability of vanadium redox species enhancing the photoresponse of a PEC even with a pristine TiO_2 photoelectrode. Furthermore, the photoelectrochemical study with a hybrid electrode, i.e., WO_3/TiO_2, showed the unique *electrochromism/photochromism* property of WO_3 as an electron storage reservior to store solar energy in certain conditions. Such energy storage ability is realized through the formation of tungsten bronze by WO_3 reacting with electrons and protons in an electrochemical system under solar illumination.

In light of that, we combined the energy storage ability of WO_3 with our newly developed all-vanadium photoelectrochemical storage cell to explore the possibility of photoelectrochemical solar energy conversion and storage, especially in the case of intermittent sunlight in this chapter.

The combined system incorporates the conventional PEC, a vanadium redox-flow battery (VRB), and a WO_3/TiO_2 hybrid photocatalyst. Zero-resistance ammetry (ZRA) and electrochemical impedance spectroscopy (EIS) were employed to further study photoelectrochemical response and reaction mechamism of this system in conversion and storage of solar energy under both illumination and dark. The results indicate an important synergy between electron storage and the all-vanadium electrolytes, which potentially offers great reversibility, high-capacity electron storage, and significant improvement in photocurrent.

4.2 Experiments

In a typical electrode fabrication procedure, TiO_2 and WO_3/TiO_2 hybrid (various WO_3 loadings) photoelectrodes with active area of 6.45 cm^2 were fabricated and used

throughout the experiment. To fabricate TiO_2 and hybrid electrodes, 1.00 g Degussa P25 TiO_2 (VP AEROPERL® by Evonik), 2.50 g α-terpineol (laboratory grade, Fisher Scientific USA) were mixed under constant stirring at 80°C for 1 hr to obtain a uniform TiO_2 or hybrid slurry with the addition of tungstic acid (Alfa Aesar USA). Then the slurry was deposited on a pre-cut square-shaped fluorine doped tin oxide (FTO) (Pilkington USA) using a doctor blade. The FTO substrate was pre-washed with acetone (99.7%, Fisher Scientific USA), methanol (99.8%, Fisher Scientific USA), and deionized (DI) water, before being blow-dried and then further dried in an oven at 120°C for 1 hr. The obtained coating was subsequently calcined with air flow at 500°C for 90 min.

Three types of electrolytes, 3 M H_2SO_4, 0.01 M vanadium(IV, VO^{2+}) in 3 M H_2SO_4, and 0.01 M vanadium(III, V^{3+}) in 3 M H_2SO_4, were used in the experiments. The first two electrolytes were prepared by dissolving H_2SO_4 (96.6%, J.T. Baker USA) in DI water with or without vanadium(IV) sulfate oxide hydrate ($VOSO_4 \cdot xH_2O$) (99.9%, Alfa Aesar USA). The number of water in $VOSO_4 \cdot xH_2O$ was determined by thermogravimetric analysis. The prepared vanadium(IV)-sulfuric acid solution appeared light blue. The 0.01 M vanadium(III) electrolyte was obtained by electrochemically reducing the prepared vanadium(IV)-H_2SO_4 solution in an electrolytic cell at constant current density of 3 mA/cm^2 using a potentiostat (Princeton Applied Research, PARSTAT 2273) until the potential reached 1.6 V. During the reduction, the electrolyte was protected by N_2 to prevent oxidation of the vanadium(III) species. The obtained vanadium(III)-sulfuric acid solution appeared light green.

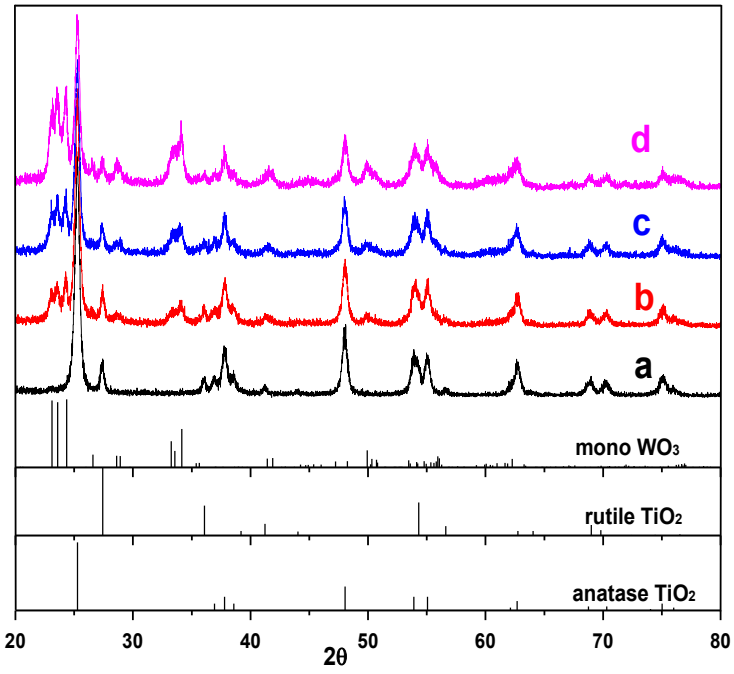

Figure 4-1 XRD spectra of (a) TiO_2 electrode, and hybrid electrodes with various WO_3 loadings: (b) 6 wt%, (c) 12 wt%, and (d) 24 wt%.

The crystallographic information of all electrodes was determined by XRD (Siemens, 810-M340-32-C3000) at a scan rate $0.01^{\circ}s^{-1}$ between 20°-80° with a dwell time of 1 s. No impurity other than anatase phase and rutile phase TiO_2, and monoclinic WO_3 was discovered from the XRD spectra (Figure 4-1).

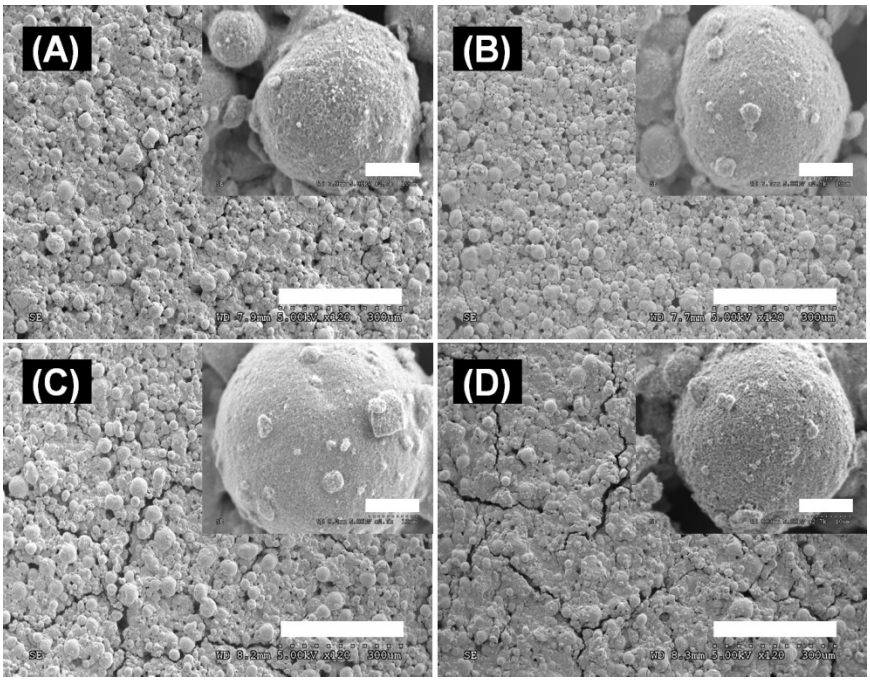

Figure 4-2 SEM images of (A) TiO_2 electrode and hybrid electrodes with different WO_3 loadings (B) 6 wt%, (C) 12 wt%, and (D) 24 wt%. High-magnification images are shown in the inset for each figure. The scale bars in low-magnification and high-magnification images represent 300 um and 10 um respectively.

Scanning electron microscopy (Hitachi S-3000 N variable pressure SEM) was used to examine the microstructure of all electrodes. The obtained SEM images (Figure 4-2) clearly show small WO_3 clusters on TiO_2 particles and mud cracks at higher WO_3 loadings, which was in agreement with our previous findings.[36, 43]

Raman spectra were collected using a PerkinElmer DXR Raman microscope from 100 to 2000 cm^{-1}. In the Raman spectra (Figure 4-3), no other peaks other than anatase TiO_2 and monoclinic WO_3 were observed. Five Raman active modes near 146, 197, 397, 515, and 633 cm^{-1} are assigned to characteristic vibration of anatase TiO_2.[43]

The peaks near 270, 326, 713 and 806 cm^{-1} belong to characteristic vibration modes of monoclinic WO_3.

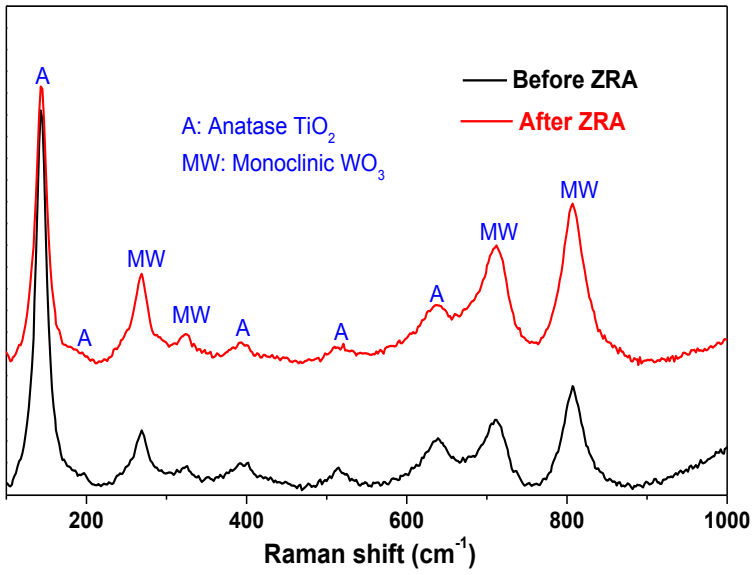

Figure 4-3 Raman Spectra of the hybrid electrode (24 wt% WO_3) before and after ZRA experiments in 3 M H_2SO_4 electrolyte.

The photoelectrochemical property of all electrodes was studied by CV, ZRA and EIS in a two-chamber, three-electrode electrochemical cell, where the photoelectrode served as the working electrode (WE), a platinum mesh and Ag/AgCl electrode served as the counter electrode (CE) and reference electrodes (RE), respectively. Details of the experimental setup have been described in our previous work.[43, 44] Tests using zero-resistance ammetry (ZRA) were conducted up to almost 4 hrs with either 3 M H_2SO_4 or 0.01 M vanadium in 3 M H_2SO_4 electrolyte under dark and AM 1.5 conditions. In a typical experiment, 3 M H_2SO_4 solution or 0.01 M V(IV) in 3 M H_2SO_4 was used as the anolyte, and 3 M H_2SO_4 solution or 0.01 M V(III) in 3 M H_2SO_4 was used as the catholyte in two chambers of the photoelectrochemical cell (PEC) separated by a Nafion 117 membrane.

Solar irradiation was created using an ozone-free solar simulator system (Newport USA) coupled with an AM 1.5 global filter (Newport USA) and calibrated using a standard photodiode (Newport USA). The electrochemical impedance spectroscopy (EIS) measurements in this study were performed on the electrochemical cell using either a TiO_2 or a hybrid electrode (24 wt% WO_3) under dark/AM1.5 illumination conditions. All data were recorded at open-circuit voltage (OCV) over a frequency range from 10 mHz to 2 MHz with an amplitude of 10 mV.

4.3 Zero-resistance Ammetry Study

We previously investigated the ability of WO_3 as an electron reservoir to store solar energy in an all-vanadium photoelectrochemical cell.[36, 43] Such energy storage ability of WO_3 is believed to be enabled through certain electrochemical conditions. However, our previous work only focused on revealing the photoelectrochemical behavior of WO_3 and WO_3/TiO_2 hybrid electrodes under light for short period of time (up to 3 min) and therefore may not reflect long-term behavior of the cell. In addition, it is unclear if the energy storage behavior of the system is reversible. To this end, prolonged photoelectrochemical study (up to almost 4 hrs) was conducted by ZRA to investigate the overall cell performance in terms of electron storage using two distinct electrolytes.

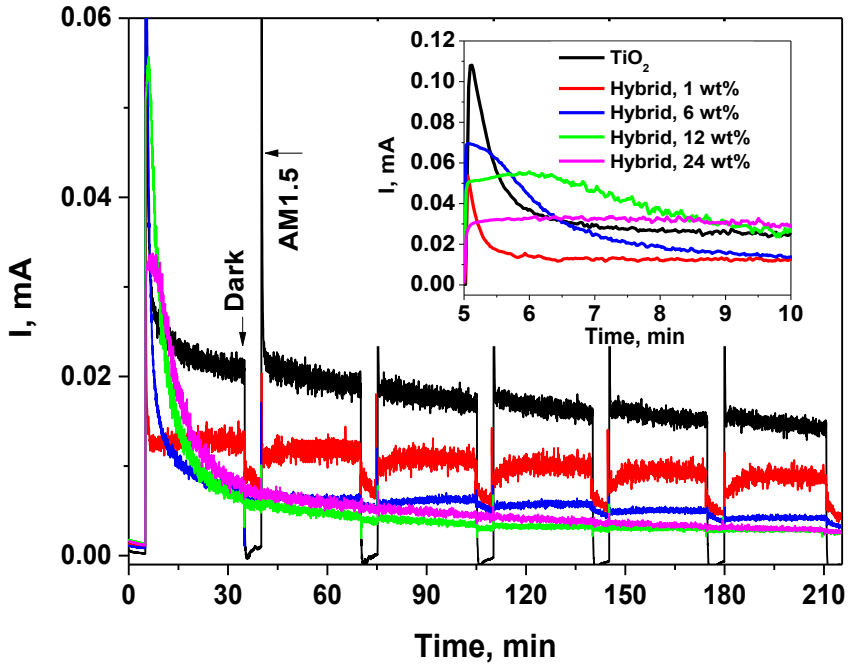

Figure 4-4 Photocurrent measurements of PECs with different electrodes in 3 M H_2SO_4 electrolytes under alternative dark/illumination conditions. The inset graph shows the photocurrent of different electrodes from 5 to 10 min under illumination.

Figure 4-4 depicts the photocurrent of different electrodes in 3 M H_2SO_4 electrolyte under alternative dark/illumination conditions and the inset graph magnifies the photoresponse from 5 to 10 min under illumination. Generally, all electrodes show relatively small photocurrent under AM 1.5 illumination, which is an indication of sluggish reaction kinetics of H_2 and O_2 evolution. Compared to the TiO_2 electrode, the hybrid electrodes show even inferior photocurrent within almost the entire test window, though it has been observed that increasing loading of WO_3 in the hybrid electrodes resulted in a red shift of absorption shoulder occurred near 450 nm.[36]

However, the inset graph indicates higher photocurrent for the hybrid electrode with 12 wt% of WO_3 than that of TiO_2 electrode during the first 5 min illumination, which is

consistent with our previous findings.[43] In addition, the photocurrents produced by the hybrid electrodes appear to reach saturation/stabilization eventually when the fraction of WO_3 is no less than 6 wt% in despite of illumination.

On the other hand, the hybrid electrodes give much more appreciable dark current (at least one order of magnitude higher) than TiO_2 electrode. Unlike the negligible dark current by TiO_2, the one by the hybrid electrodes remains almost without any decay through each dark period (5 min). These findings achieved in prolonged test seem contradictive to our previous results observed in short-time tests, but can be well explained through the reversible intercalation/de-intercalation of electrons and H^+ ions into/out of WO_3 to form hydrogen tungsten bronze, H_xWO_3. This is clearly seen from the appearance of all hybrid electrodes (Figure 4-5) before and after the photoelectrochemical experiments. The deeply colored blue-black hydrogen tungsten bronze appeared on all hybrid electrodes after AM 1.5 irradiation except the one with 1 wt% WO_3.

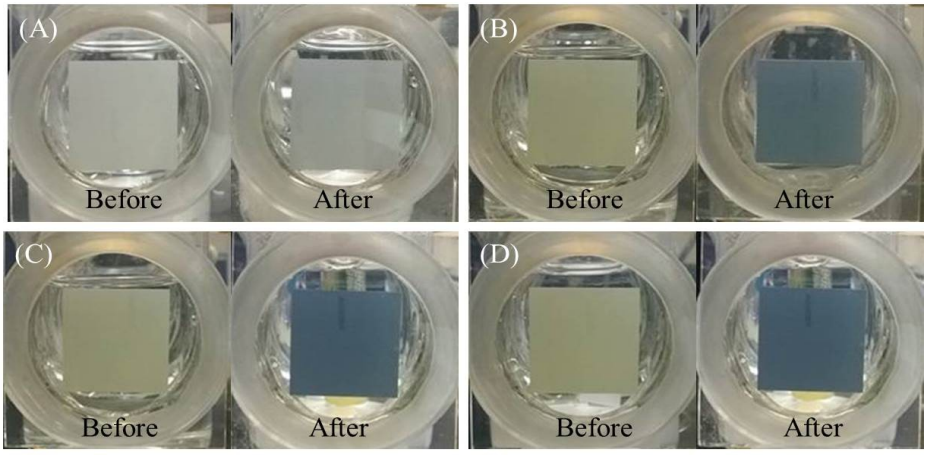

Figure 4-5 Appearance of hybrid WO_3/TiO_2 electrodes with WO_3 loadings of (A) 1 wt%, (B) 6 wt%, (C) 12 wt%, and (D) 24 wt% before and after ZRA experiment in 3 M H_2SO_4 electrolytes.

This observation coincides strongly with the photocurrent profiles of all hybrid electrodes in Figure 4-4. When light was shed on the hybrid electrode, the photogenerated electrons, apart from recombining with holes at the semiconductor/liquid interface, have higher tendency to react with WO_3 along with H^+ ions to form H_xWO_3. These H_xWO_3, scattered/distributed across the WO_3/TiO_2 matrix, are highly light-reflecting due to their metallic or quasi-metallic nature[45-47] and believed to act as a hurdle to electron transport and thus the photocurrent was reduced. This is especially clear when the photocurrent collected by the hybrid electrodes was examined. When WO_3 content in the hybrid electrode is less dominant (e.g., 1 wt%), the photocurrent is only slightly mitigated even under long-term illumination test. However, the photocurrent was reduced to saturation/stabilization once the WO_3 loading is more than 1 wt% regardless of dark/illumination conditions. The noticeable dark currents from the hybrid electrodes are due to the released electrons from decomposition reaction of hydrogen tungsten bronze. However, the reaction kinetics of such electron release is believed to be very sluggish in pure acid, resulting in unchangeable dark currents for the hybrid electrodes especially with high WO_3 loading.

Material characterization such as Raman spectroscopy and XRD was performed on the hybrid electrode (24 wt%) before and after ZRA experiments to confirm the formation of H_xWO_3. Raman spectra does not reveal observable difference on the electrode whereas XRD results (Figure 4-6) on the other hand, show structural changes of the hybrid electrode (24 wt%) after the ZRA tests.

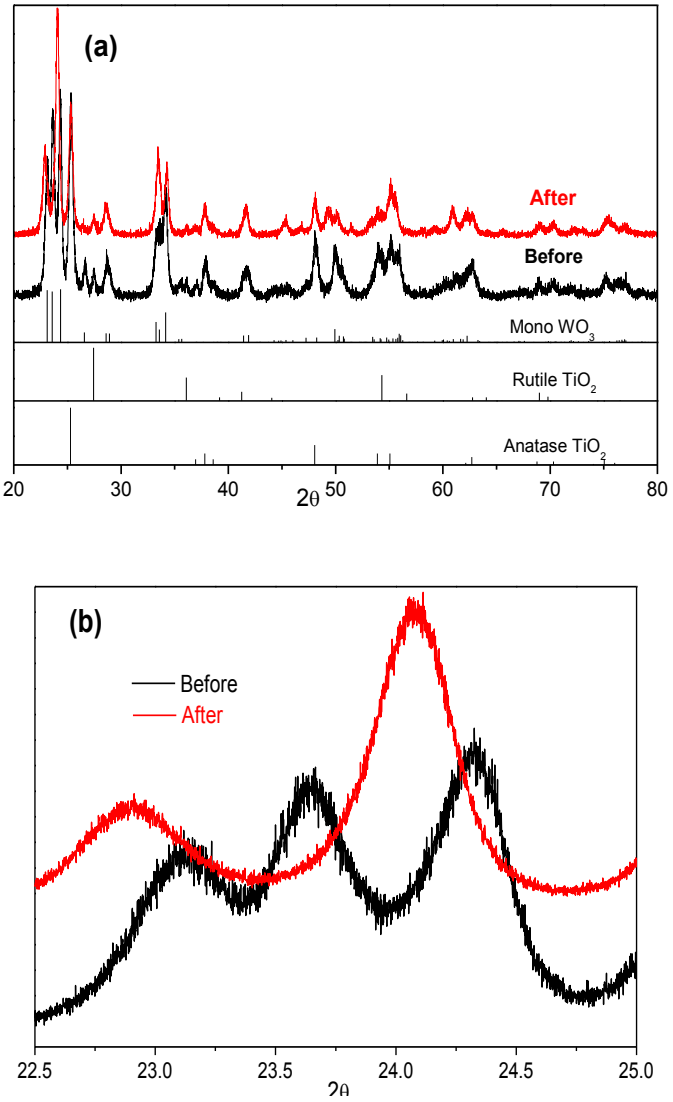

Figure 4-6 XRD spectra of the hybrid electrode (24 wt% WO_3) in the range of (a) 20 – 80° (2θ) and (b) 22.5 - 25° (2θ) showing WO_3 characteristic peaks before and after ZRA experiments in 3 M pure acid electrolyte.

In Figure 4-6A, only peaks of anatase TiO_2 (JCPDS #21-1272), rutile TiO_2 (JCPDS #76-1940), and monoclinic WO_3 (JCPDS #83-0950) were found in the sample before ZRA experiment. However, the crystal structure of WO_3 in the sample changed

from monoclinic to cubic perovskite[48, 49] after intercalation of hydrogen ions into WO_3 lattice. The major structural change appears mostly on three characteristic peaks of monoclinic WO_3 from 22.5° to 25° (Figure 4-6B) though other peaks remain the same after the formation of H_xWO_3. It is clear that not only three major WO_3 characteristic peaks disappear, but also two new peaks emerge in different positions. Dickens[48] reported that when hydrogen ions are inserted into WO_3 lattice, all the corner-shared WO_6 octahedra are tilted relative to the orientation that is expected in a perovskite structure. Thus, it is believed that such WO_6 octahedra tilt is responsible for the observed structural change of the hybrid electrode before and after the formation of H_xWO_3 in this study.

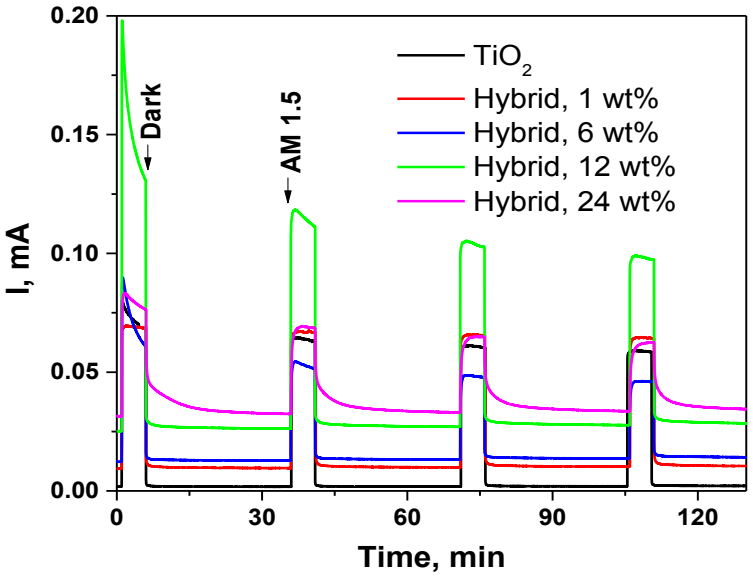

Figure 4-7 Photocurrent measurements of PECs with different electrodes in 0.01 M all-vanadium electrolytes under alternative dark/illumination conditions.

The photocurrents collected from various electrodes in Figure 4-7 when 0.01 M all-vanadium electrolytes were used, are significantly different from what is shown in Figure 4-4. The TiO_2 electrode demonstrated distinctly different photoelectrochemical

behavior than the hybrid ones. All hybrid electrodes show much higher photocurrent in all-vanadium electrolyte compared to those in pure acid electrolyte. The improvement on photocurrent is attributed to mitigated charge carrier recombination and fast reaction kinetics of vanadium redox species. In addition, the amount of WO_3 in the hybrid electrode was discovered to play an important role affecting the photoelectrochemical behavior of electrodes. When WO_3 content in hybrid electrode was either inadequate or abundant, the photocurrent was mitigated compared to that of TiO_2 and only medium WO_3 loading (12 wt%) in the hybrid electrode gave optimum photocurrent. This observation can be ascribed to the competition among vanadium redox reactions, charge carrier recombination, and tungsten bronze formation reaction at the semiconductor/liquid interface. When vanadium redox species were involved in the electrolyte, the photoelectrons preferentially participated in redox reactions in addition to those in forming hydrogen tungsten bronze, due to fast reaction kinetics of vanadium species and the narrow-band-gap WO_3. It is deduced that the charge carrier recombination reaction dominates over the other reactions when WO_3 loading is insignificant; whereas WO_3 may induce charge trapping effects in the bulk[50] and form more hydrogen tungsten bronze when its loading is too high. An optimum amount of WO_3 in the hybrid electrodes serves as a mediator for effective charge carrier separation by minimizing the recombination losses with the assistance of vanadium redox species during illumination.

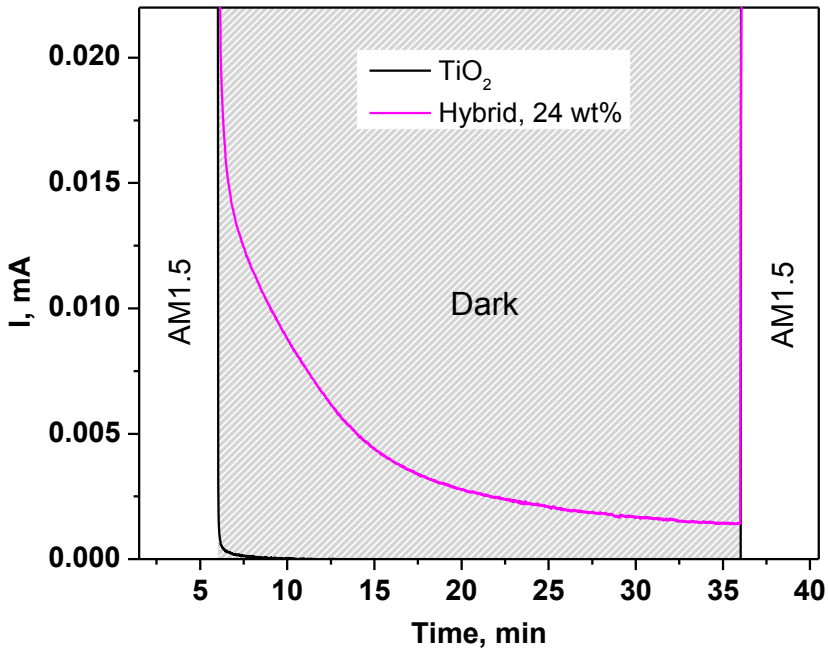

Figure 4-8 Significant electron storage capacity of the hybrid electrode (24 wt% WO_3) compared to the TiO_2 electrode in 0.01 M all-vanadium electrolytes after the first 5 min illumination. The graph was rearranged from Figure 4-7.

On the other hand, the ability of the hybrid electrodes to store photogenerated electrons compared to TiO_2 is conspicuously manifested in all-vanadium electrolytes by their dark current shown in Figure 4-7 and Figure 4-8. Note that the test protocol shown in the graph was slightly adjusted from that in Figure 4-4 to better exhibit the significant dark currents of the hybrid electrodes under illumination according to our preliminary experiments. In Figure 4-7, the hybrid electrodes were found to release electrons under dark condition for prolonged periods of time and the dark current was almost linearly proportional to the amount of WO_3 in the hybrid electrodes.

The hybrid electrode with 24 wt% WO_3 exhibits substantial electron storage capacity under dark (estimated to be 0.299 mAh/g or 1.078 C/g) in the form of prolonged

electron release up to 30 min (Figure 4-8) with only 5-min illumination. The released electrons from the hybrid electrodes under dark are believed due to decomposition of hydrogen tungsten bronze formed during illumination and they can be used to continue reducing the vanadium redox species even under dark. In other words, the photoelectrochemical cell could keep being charged even under dark condition and this may open a new perspective for photoelectrochemical solar energy conversion and storage.

4.4 Electrochemical Impedance Spectroscopy Study

As exhibited in Figure 4-4 and Figure 4-7, hydrogen tungsten bronze formed under illumination is believed to block the semiconductor/electrolyte interface and thus compromise the photocurrent. It is crucial then to study the charge transfer at the interface between the photoelectrode and electrolyte before, during and after the illumination to understand its implication to photoelectrochemical kinetics.

Electrochemical impedance spectroscopy (EIS) is one of the most powerful techniques for investigating charge transfer processes in an electrochemical device. To this end, EIS measurement was conducted at OCV of the cells on different photoelectrodes under dark/illumination conditions. Figure 4-9 and Figure 4-10 represent the Nyquist plots of the TiO_2 and hybrid (24 wt% WO_3) electrodes, respectively, in pure acid or 0.01 M all-vanadium electrolytes under dark and illumination conditions. As shown in Figure 4-9 and Figure 4-10, TiO_2 and hybrid electrodes show distinct characteristics of impedance in two electrolytes albeit their spectra are all composed of similar arcs/partial arcs. Generally, an arc in the Nyquist plot represents existence of an electrochemical interface and the appearance of plural arcs indicates different time constants of electrochemical interfaces for electron transport in the electrochemical system.

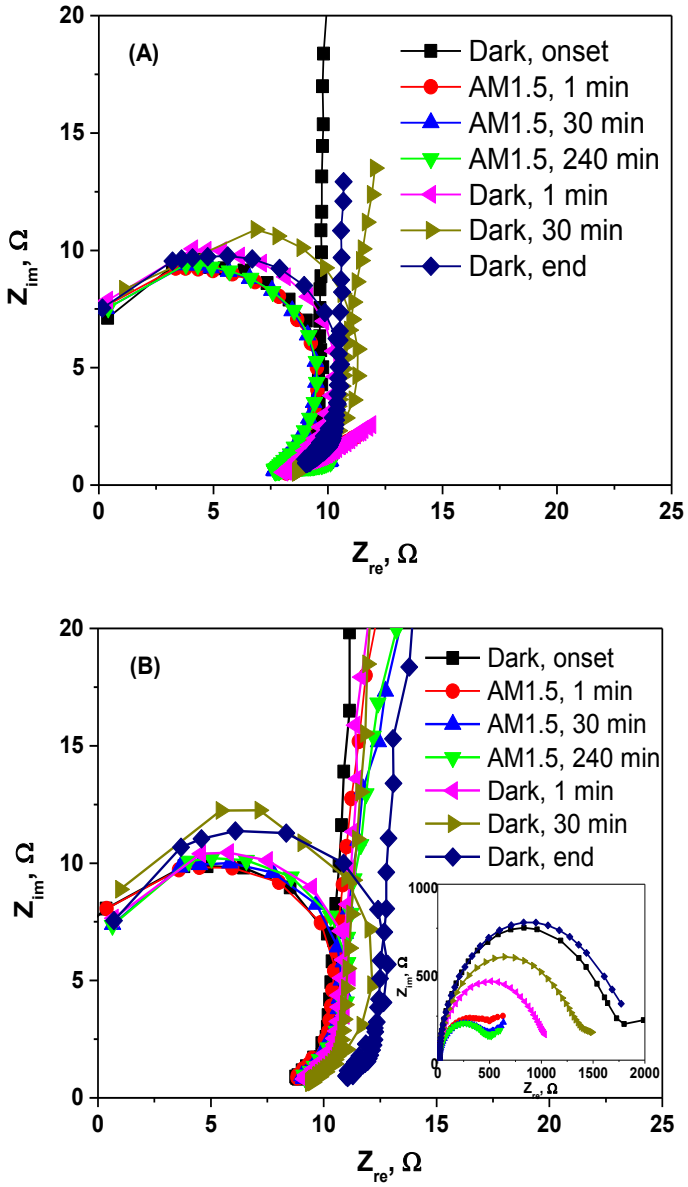

Figure 4-9 Nyquist plots of PECs in (A) 3 M H_2SO_4 and (B) 0.01 M all-vanadium with a TiO_2 photoelectrode. The inset graph in Figure 4-9B represents Nyquist plots of the cell in all tested frequency.

When only 3 M H_2SO_4 electrolyte was used (Figure 4-9A), the high-frequency arc and an even bigger arc (only a portion) at low frequency, according to consensus in

literature,[51, 52] are believed to correspond to electron transport resistance and interfacial capacitance at Pt/electrolyte and TiO_2/electrolyte interface, respectively. The dominantly large diameter of the low-frequency arc indicates huge charge transfer resistance and thus sluggish reaction kinetics[53] regardless of illumination. This finding corroborates with the observation in Figure 4-4, indicating water splitting by TiO_2 is intrinsically sluggish. Note that the diameter of the small arc at high frequency is independent of dark/illumination conditions, proving that no change occurred on Pt electrode itself.

However, when vanadium redox species were involved in the electrolyte (Figure 4-9B) and new interfaces were created, big difference is seen on impedance spectra compared to Figure 4-9A. One more arc with much larger diameter emerged at mid frequency and it represents the charge transfer resistance and interfacial capacitance at TiO_2/vanadium(IV) redox interface. The new arc at mid frequency dominates much more in the whole impedance spectra than electron transport at high frequency and Warburg diffusion resistance at low frequency. Though not fully understood, this result indicates that vanadium redox plays a vital role at TiO_2/vanadium(IV) redox and Pt/vanadium(III) redox interfaces in terms of charge transfer resistance and electron transport resistance.

In addition, the new interfaces created by vanadium redox species seem to have little influence on electron transport resistance at the counter electrode as the resistance values (see magnified inset graph in Figure 4-9B are very similar to their counterparts in Figure 4-9A regardless of dark/illumination conditions.

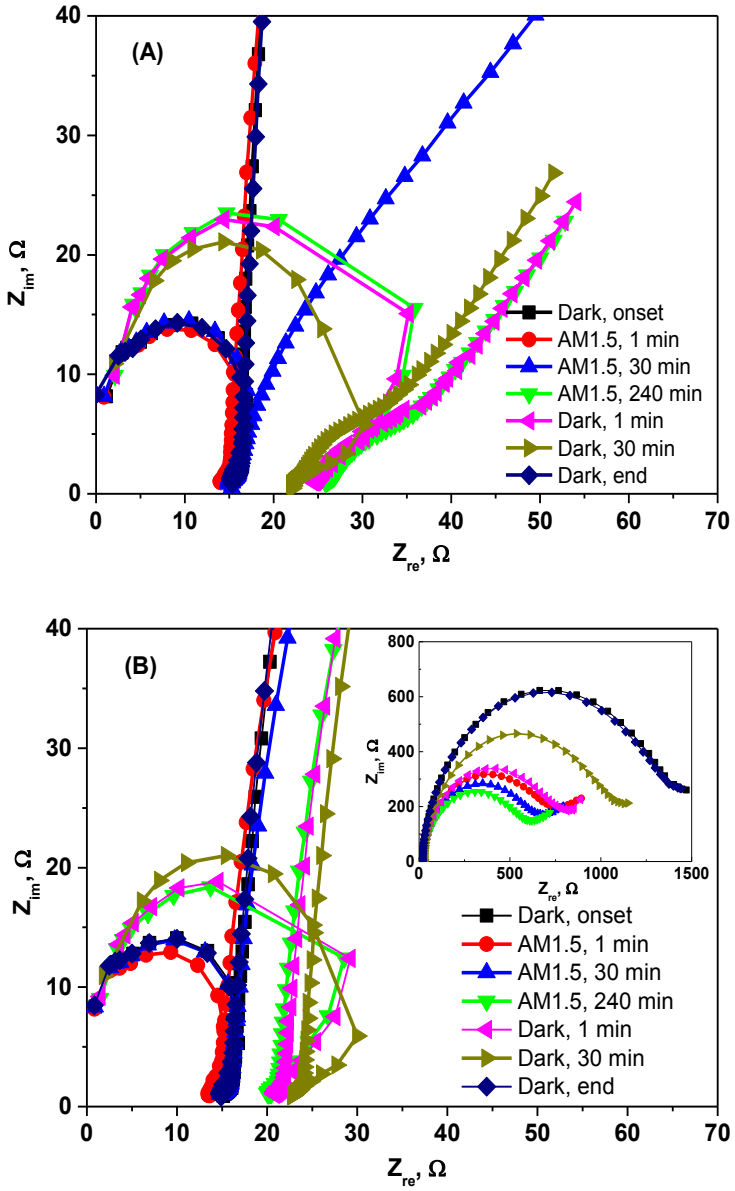

Figure 4-10 Nyquist impedance spectra of PECs in (A) 3 M H_2SO_4 electrolytes and (B) 0.01 M all-vanadium electrolytes with a hybrid (24 wt% WO_3) photoelectrode. The inset graph in Figure 4-10B represents Nyquist plots of the cell under various conditions in all tested frequencies.

However, the charge transfer resistance with vanadium redox species was considerably reduced up to three times under AM 1.5 illumination. This is due to facilitated electron generation and transport by fast reaction kinetics of vanadium redox, which is in agreement with Figure 4-7. As indicated in our previous study,[43] the vanadium redox also shifts the dynamic balance between charge carrier recombination and redox reaction toward the latter, which is verified in Figure 4-9B. The electron transport resistance (diameter of the mid-frequency arc) after illumination for 1 min (red line) was greatly reduced and quickly reached stabilization in 30 min (blue line). The EIS spectra remained unchanged even up to 4 hrs (green line). Besides, when the light was turned off, the electron transport resistance was promptly increased and reverted back to its original value as before the test. Comparison between Figure 4-9A and Figure 4-9B clearly reveals the quick charge transfer at the semiconductor/electrolyte interface when vanadium redox species were employed.

Figure 4-10 depicts the Nyquist plots of the hybrid (24 wt% WO_3) electrode in the photoelectrochemical cell using two electrolytes. They have similar characteristic arcs/diffusion components as those of TiO_2 in Figure 4-9, but with some obvious differences. As suspected from Figure 4-4, hydrogen tungsten bronze formed under illumination by WO_3 reacting with photogenerated electrons and H^+ ions in the electrolyte is realized as a hurdle to electron transport at the semiconductor/electrolyte interface. Such speculation is confirmed from the impedance spectra shown in Figure 4-10. The electron transport resistance corresponding to the Pt/electrolyte interface (i.e., diameter of the high-frequency arc) in both electrolytes was nearly doubled under illumination and this increase was strictly dependent on time.

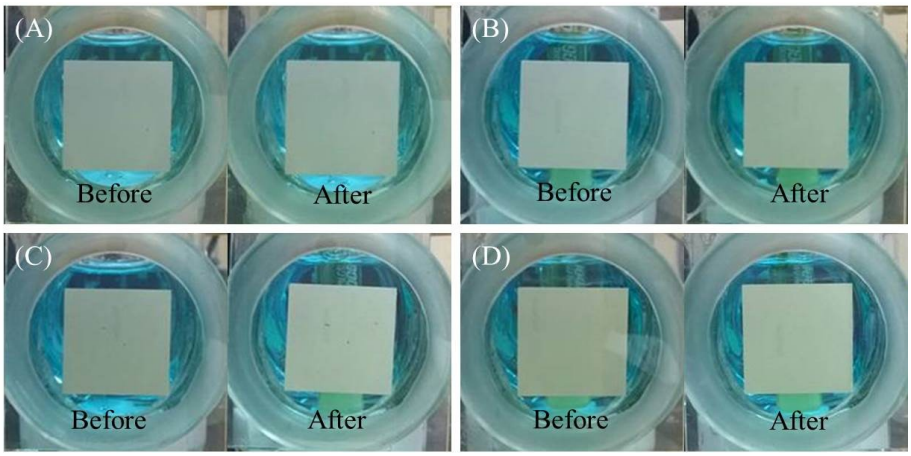

Figure 4-11 Appearance of hybrid WO_3/TiO_2 electrodes with WO_3 loadings of (A) 1 wt%, (B) 6 wt%, (C) 12 wt%, and (D) 24 wt% before and after ZRA experiment in 0.01 M all-vanadium electrolytes.

Though the nature of the Pt/electrolyte interface at the counter electrode remained unchanged; however, the charge transfer kinetics might be impeded under illumination because the incoming electrons from the photoelectrode are blocked by the formation of H_xWO_3. It is seen in Figure 4-10B that an increase in electron transport resistance, as a result of H_xWO_3 formation, appeared delayed in all-vanadium electrolytes. Besides, the electron transport resistance after long-term illumination (4 hrs) was about 5 Ω lower than that in 3 M H_2SO_4 electrolytes. Such results are consistent with the observed saturated photocurrent of the hybrid (24 wt%) electrode in Figure 4-4, and the electrode appearance change in Figure 4-5 and Figure 4-11. It is believed that fast reactions of vanadium(IV) redox species at the photoelectrode surface, which quickly consume the photogenerated electrons, leave only a small fraction of those to participate in the formation of H_xWO_3. This significantly delays growth of H_xWO_3 on the photoelectrode and results in slow changes of both high-frequency and mid-frequency arcs in Figure 4-10B. The above analysis was confirmed by the unchanged electrode

appearance (Figure 4-11) for different WO_3 loadings in 0.01 M all-vanadium electrolyte before and after the test.

4.5 Electron Storage Mechanism

To better understand the observed EIS spectra of the hybrid electrode in two electrolyte systems under different dark/illumination conditions, a model based upon the relevant electronic states of different components and standard electrochemical potential of different vanadium redox species is proposed in Figure 4-12.

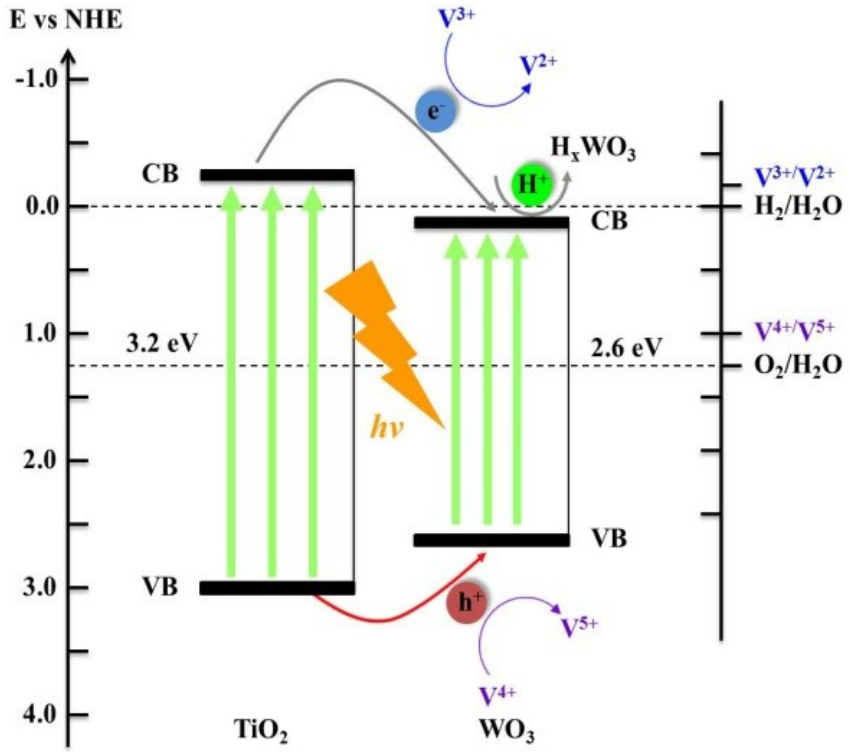

Figure 4-12 Schematic representation of proposed electron storage mechanism and charge transfer pathways for the hybrid WO_3/TiO_2 electrode in the all-vanadium photoelectrochemical storage cell.

This model also helps further elucidate the electron storage mechanism and charge transfer pathway for the hybrid electrode. In this model, to avoid unnecessary ambiguity, the bandgap energy of WO_3 is designated as 2.6 eV and the conduction band (CB) edge is about 0.4 V more positive than that of TiO_2 in the electrochemical scale as is typically reported in literatures.[54-59] Although controversy remains in the academic society that the bandgap energy of WO_3 spans from 2.6 to 3.3 eV. However, these values mainly differ in the position/maximum energy level of valence band (VB) and thus shall have little impact in our discussion regarding the electron storage mechanism for the hybrid electrode and charge carrier transfer processes.

As illustrated in Figure 4-12, the photogenerated electrons and holes in TiO_2 need to travel "downhill" and "uphill" to the CB and VB of WO_3 respectively because of their relative band positions. The more positive CB and more negative VB of WO_3 are deemed as the driving force for such charge carrier migration. During this process, different reaction scenarios emerge depending on the electrolyte used. When pure acid was employed as the electrolyte, photogenerated holes from TiO_2 and WO_3 oxidize H_2O to result in O_2 evolution while the photoelectrons react with WO_3 and H^+ ions to form hydrogen tungsten bronze. This is why the blue-black coloration appeared on the electrodes after illumination in pure acid electrolyte. Note that such photochromism highly depends on the amount of WO_3 that participates the reaction and electron transfer kinetics. When WO_3 loading in hybrid electrode is insignificant (e.g. 1 wt%), the photochromism is insignificant (Figure 4-5) as little difference was found after long-term illumination up to 4 hrs by examining the electrode appearance. However, noticeable dark current observed after switching off the light clearly indicates the formation of hydrogen tungsten bronze and its slow decomposition to release electrons. As for the hybrid electrodes with higher WO_3 loading, blue-black coloration (Figure 4-5) was

observed after the same test and the photocurrent (Figure 4-4) during the test quickly reached to saturation/stabilization regardless of dark/illumination condition. These observations confirm that (i) hydrogen tungsten bronze is preferably formed out of hybrid electrodes under AM 1.5 illumination, (ii) it renders as the barricade to prevent electron transfer, (iii) the decomposition is very slow as revealed in Fujishma's work.[39]

When vanadium redox species were involved in the electrolyte, photogenerated charge carriers, have a distinct pathway at the semiconductor/liquid interface. Similar as in the previous scenario, photogenerated holes from TiO_2 will still travel "uphill" to the WO_3 VB and join their counterparts there. Instead of evolving O_2, these holes are inclined to oxidize vanadium(IV) ions to vanadium(V) ions due to more negative electrochemical potential and faster reaction kinetics of V^{4+}/V^{5+} redox[36, 43] compared to oxygen evolution reaction. On the other hand, the photogenerated electrons from TiO_2 are speculated to mainly/completely react with vanadium(III) ions in the catholyte and reduce them to vanadium(II) ions when they travel "downhill" to the conduction band of WO_3 as a result of fast electrochemical kinetics of V^{3+}/V^{2+} redox. The remaining photogenerated electrons from TiO_2, if any, along with their counterparts in WO_3 will react with WO_3 to form hydrogen tungsten bronze. This process is reverted under dark upon demand releasing the stored electrons. This finding is confirmed by the prolonged dark current (Figure 4-7 and Figure 4-8) and EIS measurement (Figure 4.10B) as the resistance was increased after long-term illumination, which indicates the existence of hydrogen tungsten bronze.

Meanwhile, the fast reaction kinetics of V^{3+}/V^{2+} redox is believed to prevent TiO_2 photoelectrons from recombination, thus providing much higher photocurrent than that is exhibited in pure acid electrolyte. In other words, hybrid electrode is capable of revitalizing photocurrent in all-vanadium electrolytes under illumination and releasing

electron energy stored in hydrogen tungsten bronze under dark simultaneously. Note that the magnitude of photocurrent revitalized and the electron energy released strongly depend on the amount of WO_3 in hybrid electrode and redox reaction kinetics. Most important, the electron storage capability of the hybrid electrode when coupled with the all-vanadium electrolytes, in comparison with pure acid electrolytes, potentially offer great reversibility (Figure 4-11), long-term electron storage (up to 4 hrs in Figure 4-10), and significant improvement in photocurrent (Figure 4-5). Since what has been demonstrated here in this work only employed unmodified semiconductors, it is envisioned that further improvement can be brought in by future optimization to enable practically meaningful continuous solar energy conversion and storage using advanced semiconductors in tandem structure.

4.6 Conclusion

The energy storage ability of WO_3 was investigated using WO_3/TiO_2 hybrid photoelectrodes in an all-vanadium photoelectrochemical storage cell under either dark or illumination conditions. ZRA and EIS were used to probe photoelectrochemical and electrochemical behavior of the cell with respect to photoelectrochemical solar energy conversion and storage.

Results revealed mitigated photocurrent in pure acid electrolyte but enhanced photoresponse of the hybrid electrodes in all-vanadium electrolytes under long-term illumination. Without applying the bias, hydrogen tungsten bronze was formed in both pure acid and all-vanadium electrolytes, and this finding was corroborated by EIS results and material characterization results. In pure acid, the formed hydrogen tungsten bronze acts as the hurdle to prevent electron transport and thus mitigates the photocurrent, whereas all-vanadium electrolytes are beneficial to revitalize photocurrent of the hybrid electrodes under illumination and realize energy storage ability of WO_3 under dark.

However, a complicated interplay was found to exist between achieved photocurrent and released dark current by using different WO_3 loadings in the hybrid photoelectrode. A model is then proposed to elaborate the observed experimental results and the charge carrier transfer pathways. The vanadium redox species, due to their fast electrochemical kinetics, not only enhance the photocurrents under illumination through mitigating formation of H_xWO_3, but also help release reversely stored electrons under dark.

Chapter 5

Electrolyte Study of All-Vanadium PEC

5.1 Introduction

Previously, we studied the photoresponse of typical n-type photoelectrodes such as TiO_2 and WO_3/TiO_2 with the assistance of vanadium redox species. The initial results show significantly enhanced photoelectrochemical performance (15 times higher IPCE[44]) of the PEC even with an non-optimized system when vanadium redox species were added in the electrolyte.

To realize even better photocatalytic property of the PEC, optimization on cell components, e.g., electrode, membrane and electrolyte is necessary. However, the state-of-the-art electrode and membrane normally require delicate material synthesis or fabrication and laborious procedures and thus time-consuming. Replacing the electrolyte instead deems it a very fast, convenient and cost-effective approach to achieve the goal. Therefore, seeking for electrolytes especially acid-based ones with high solution conductivity, superior electrochemical activity, chemical stability and environment non-toxicity prioritizes our tasks of cell optimization for better photoelectrochemical performance.

Methanesulfonc acid (MSA) has been widely used as a commercial electrolyte standard in the past three decades to replace the previous industrial standard, fluoroboric acid in many electrochemical processes especially those involving lead and tin. This is due to its diverse physical and chemical properties such as good thermal stability, high water miscibility and metal salts solubility, low relative toxicity and high conductivity. It is already reported that the conductivity of 1.0 $mol \cdot L^{-1}$ MSA aqueous solution is 0.30 $S \cdot cm^{-1}$, comparable to that of hydrochloric acid and sulfuric acid (0.35 $S \cdot cm^{-1}$ and 0.44 $S \cdot cm^{-1}$, respectively), while posing a lower risk of corrosion compared with other mineral

acids. In addition, MSA aqueous solutions exposed to open atmospheric conditions display a unique stabilization of metal ions in their lower valence states, or, stated differently, MSA solutions allow for a unique resistance to the oxidation of metal ions to their higher valence states.

Due to these distinguished properties, using MSA as the supporting electrolyte to improve electrochemical properties has become a hot topic in flow battery research recent years.[60-64] These preliminary electrochemical studies all reveal its more pronounced metal salt solubility, redox reaction reversibility, reaction kinetics and cell efficiencies compared to conventional sulfuric acid. More recently, MSA has been employed as the electrolyte in PEC study by a group of Poland researchers[65] and their results clearly indicate long-term stability and more admirable photoelectrochemical performance achieved by MSA than H_2SO_4 and $HClO_4$ on a WO_3 nanostructured photoelectrode under the same acid concentration.

In this chapter, we investigated long-term chemical stability, bulk conductivity, electrochemical and photoelectrochemical performance of our all-vanadium PEC using MSA as the supporting electrolyte by four-point electrical conductivity measurement, CV, ZRA and EIS. The results, compared to those achieved under the same conditions using H_2SO_4 as the supporting electrolyte show its great potential to further enhance photoelectrochemical performance of all-vanadium PEC.

5.2 Experiments

TiO_2 photoelectrode with active area of 1.61 cm^2 were fabricated and used throughout the experiment. To fabricate TiO_2 electrode, 1.00 g Degussa P25 TiO_2 (VP AEROPERL® by Evonik), 2.50 g α-terpineol (laboratory grade, Fisher Scientific USA) were mixed under constant stirring at 80°C for 1 hr to obtain a uniform TiO_2 slurry. Then the slurry was deposited on a pre-cut square-shaped fluorine doped tin oxide (FTO)

(Pilkington USA) using a doctor blade. The FTO substrate was pre-washed with acetone (99.7%, Fisher Scientific USA), methanol (99.8%, Fisher Scientific USA), and deionized (DI) water, before being blow-dried and then further dried in an oven at 120°C for 1 hr. The obtained coating was subsequently calcined with air flow at 500°C for 90 min. Since the electrode fabrication process is very reproductive, material characterization results are thus referred to previous chapters.

Six types of electrolytes, 3 M H_2SO_4 or MSA, 0.01 M vanadium(IV, VO^{2+}) in 3 M H_2SO_4 or MSA, and 0.01 M vanadium(III, V^{3+}) in 3 M H_2SO_4 or MSA were used in the experiments. The H_2SO_4-based electrolytes were prepared by dissolving H_2SO_4 (96.6%, J.T. Baker USA) in DI water with or without vanadium(IV) sulfate oxide hydrate ($VOSO_4 \cdot xH_2O$) (99.9%, Alfa Aesar USA) while the MSA-based electrolytes were prepared by dissolving MSA (98%, Alfa Aesar USA) in DI water with or without vanadium(IV) sulfate oxide hydrate ($VOSO_4 \cdot xH_2O$) (99.9%, Alfa Aesar USA). The number of water in $VOSO_4 \cdot xH_2O$ was determined by thermogravimetric analysis. The prepared vanadium(IV)-sulfuric acid and vanadium(IV)-MSA solution both appeared light blue. The 0.01 M vanadium(III) electrolyte was obtained by electrochemically reducing the prepared vanadium(IV)-H_2SO_4 or vanadium(IV)-MSA solution in an electrolytic cell at constant current density of 3 mA/cm^2 using a potentiostat (Princeton Applied Research, PARSTAT 2273) until the potential reached 1.6 V. During the reduction, the electrolyte was protected by N_2 to prevent oxidation of the vanadium(III) species. The obtained vanadium(III)-sulfuric acid and vanadium(IV)-MSA solution appeared light green as well.

The photoelectrochemical property of TiO_2 electrode was studied by CV, ZRA and EIS in a two-chamber, three-electrode electrochemical cell, where the photoelectrode served as the working electrode (WE), a platinum mesh and Ag/AgCl electrode served as the counter electrode (CE) and reference electrodes (RE),

respectively. Details of the experimental setup have been described in previous chapters. Tests using zero-resistance ammetry (ZRA) were conducted with either 3 M pure acid or 0.01 M vanadium-pure acid electrolyte under alternate dark and AM 1.5 conditions. In a typical experiment, 3 M H_2SO_4 or MSA solution or 0.01 M V(IV) in 3 M H_2SO_4 or MSA was used as the anolyte, and 3 M H_2SO_4 or MSA solution or 0.01 M V(III) in 3 M H_2SO_4 or MSA was used as the catholyte in two chambers of the PEC separated by a Nafion 117 membrane.

Solar irradiation was created using an ozone-free solar simulator system (Newport USA) coupled with an AM 1.5 global filter (Newport USA) and calibrated using a standard photodiode (Newport USA). The electrochemical impedance spectroscopy (EIS) measurements in this study were performed on the electrochemical cell using a TiO_2 electrode under dark/AM 1.5 illumination conditions. All data were recorded at open-circuit voltage (OCV) over a frequency range from 1 mHz to 2 MHz with an amplitude of 10 mV.

5.3 Cyclic Voltammetry and Zero-resistance Ammetry Study

Cyclic voltammetry was employed to investigate the chemical stability of methanesulfonic acid while the PEC was in operation. Figure 5-1 shows the cyclic voltammogram of the PEC using pure MSA as the electrolyte in conjunction with a TiO_2 photoelectrode under a large scan range. Fifty scans were conducted on the PEC under alternate dark and AM 1.5 illumination conditions. As shown in Figure 5-1, TiO_2 shows a typical n-type semiconductor photoelectrochemical behavior in MSA electrolyte. Under the scan range, no other oxidation/reduction peak other than the apparent one near -0.11 V is observed on anodic scans. This peak is ascribed to charge compensating proton adsorption or intercalation reaction on TiO_2 in acidic aqueous electrolyte[66-68] and is described schematically by the *brutto* reaction:

$$Ti^{IV}O_2 + e^- + H^+ \leftrightarrow Ti^{III}(O)(OH) \text{.....5.1}$$

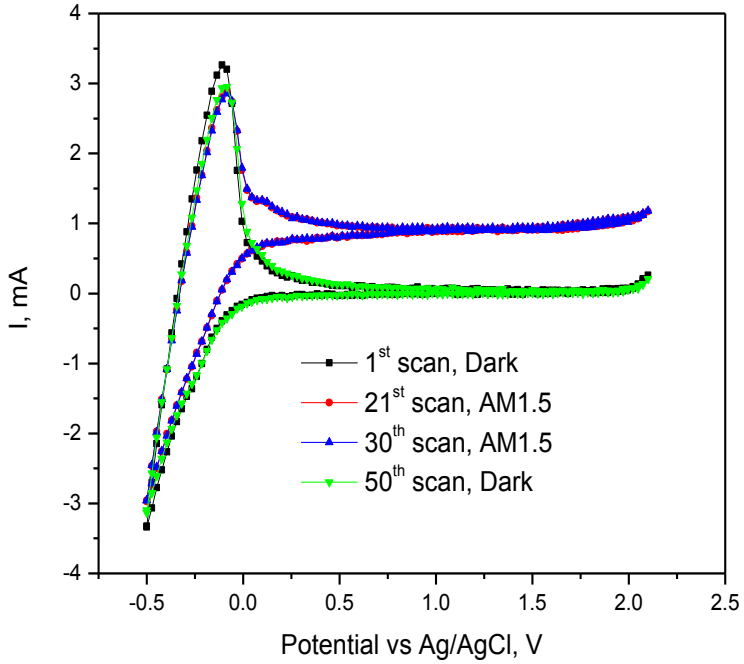

Figure 5-1 Cyclic voltammetry of a PEC using pure MSA as the electrolyte and TiO_2 as the photoelectrode with scan range of -0.5 to 2.1V under dark and AM 1.5 illumination. The scan rate was 20 mV/s.

In addition, above 2.0 V, the current starts to increase rapidly due to sufficient overpotential being provided to split water with fast reaction rate, either electrolytically (under dark) or photoelectrolytically (under AM 1.5). The CV results shown in Figure 5-1 confirm that MSA is a chemical stable electrolyte to participate in electrochemical and photoelectrochemical reactions.

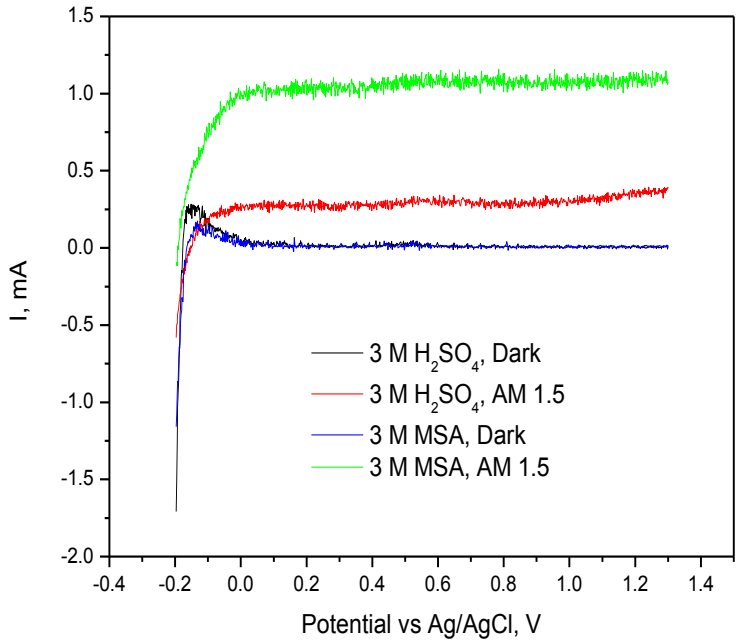

Figure 5-2 Linear sweep voltammetry of a PEC using TiO_2 as the photoelectrode in 3 M H_2SO_4 and 3 M MSA electrolytes under dark and AM 1.5 illumination.

Figure 5-2 compares photoelectrochemical performance of a TiO_2 photoelectrode in 3 M H_2SO_4 and 3 M MSA electrolytes under dark and AM 1.5 illumination by linear sweep voltammetry. It is shown that MSA improves photocurrent significantly than H_2SO_4 at the same concentration on the TiO_2 photoelectrode and a four-fold improvement in photocurrent was achieved. Considering the fact that the concentration of MSA used in our experiments are very high, i.e., negative pH value of the electrolyte, the above preliminary results render MSA a very promising electrolyte compared to conventional H_2SO_4 for photoelectrochemical solar energy conversion and storage.

However, these results rely on cyclic voltammetry that requires an external bias applied to the cell. In order to further investigate photoelectrochemical performance of MSA with more practical meaning, ZRA method (no applied external bias) was conducted

on TiO_2 photoelectrode in various electrolytes with or without the support of vanadium redox, and the results are shown in Figure 5-3. As seen in Figure 5-3, pure MSA is chemically stable upon illumination and shows clearly enhanced photocurrent (5 times higher) than pure H_2SO_4 over the entire test window under AM 1.5 illumination. Albeit current spikes, attributed to surface trap states of TiO_2 were observed at the beginning upon each illumination, the photocurrent reaches equilibration eventually after short period of time. This result is in alignment with above CV findings and it further justifies MSA being a promising electrolyte for the photoelectrochemical solar energy conversion and storage. What seems interesting in Figure 5-3 is that and MSA gives higher photocurrent on a TiO_2 photoelectrode even than 0.01 M V in 3 M H_2SO_4 electrolyte, which might indicate higher diffusion coefficient of electroactive species in the former compared to the latter. It is suspected that 0.01 M V in 3 M MSA would show even more enhanced photoelectrochemical performance when vanadium redox is involved in the electrolyte. Such speculation is confirmed by green line in Figure 5-3. When vanadium is involved in the electrolyte, the photocurrent of TiO_2 in V-MSA electrolyte is boosted more than 6 times than that in V-H_2SO_4 electrolyte under the same concentration after it is stabilized. Note that there are two different ZRA profiles using the same TiO_2 photoelectrodes emerging in various electrolytes. The ZRA profile using H_2SO_4, V-H_2SO_4 and V-MSA resemble with each other, showing gradually increased photocurrent till equilibration upon illumination while ZRA profile using MSA shows gradually dropped photocurrent till equilibration upon illumination. In our preliminary experiments, we discovered that ZRA profile using MSA also shows a gradually increased photocurrent at the beginning upon illumination. However, the increased photocurrent starts to drop abruptly till equilibration after certain period of time. Thus it is more scientific to use ZRA profile of the electrolyte after the photocurrent reaches to equilibration. Meanwhile, the

ZRA profiles using MSA and V-MSA electrolytes both show residual dark current in Figure 5-3. Such dark current is believed to be due to uncompensated charge carrier adsorption at the semiconductor/liquid interface immediately after light off. These uncompensated charge carriers can be eliminated by discharging the PEC under dark for long period of time according to our experiments (not shown here).

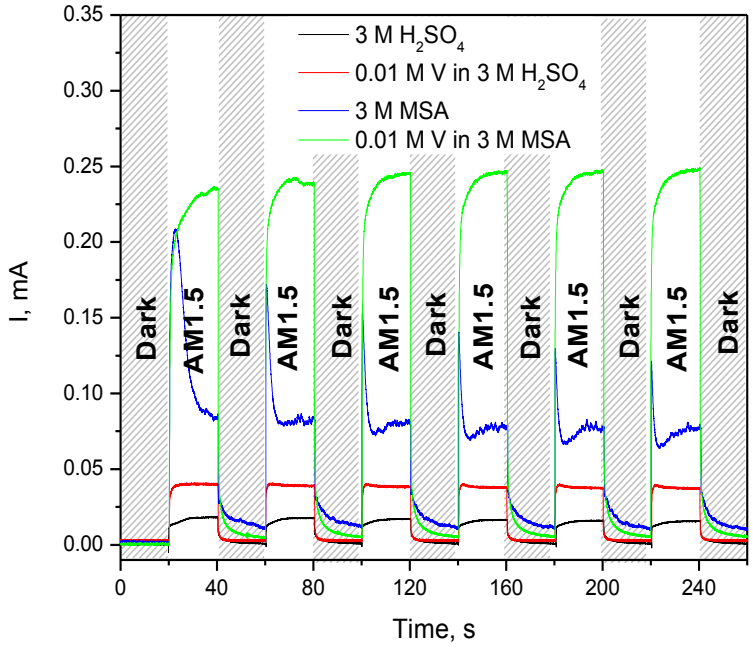

Figure 5-3 Photocurrents of TiO_2 photoelectrode using ZRA method in various electrolytes under alternate dark and AM 1.5 illumination conditions.

As demonstrated by both CV and ZRA experiments, MSA is much more superior electrolyte compared to H_2SO_4 in terms of both photoelectrochemical performance and chemical stability. However, the root cause of its better performance over H_2SO_4 remains unknown to us, so it is crucial to investigate electrochemical and photoelectrochemical reaction kinetics and mechanism to unfold the fundamentals behind.

5.4 Bulk Ionic Conductivity Study

We started first by studying bulk ionic conductivity of the electrolyte using electrochemical impedance spectroscopy and four-probe electrical conductivity measurement. The Nyquist plot of a homemade test cell using various electrolytes are shown in Figure 5-4. Four different electrolytes were tested and all samples show very similar semi-circle indicating the interface between the electrode and the electrolyte. The interception of these semi-circles on Y=0 gives ohmic resistance of the cell.

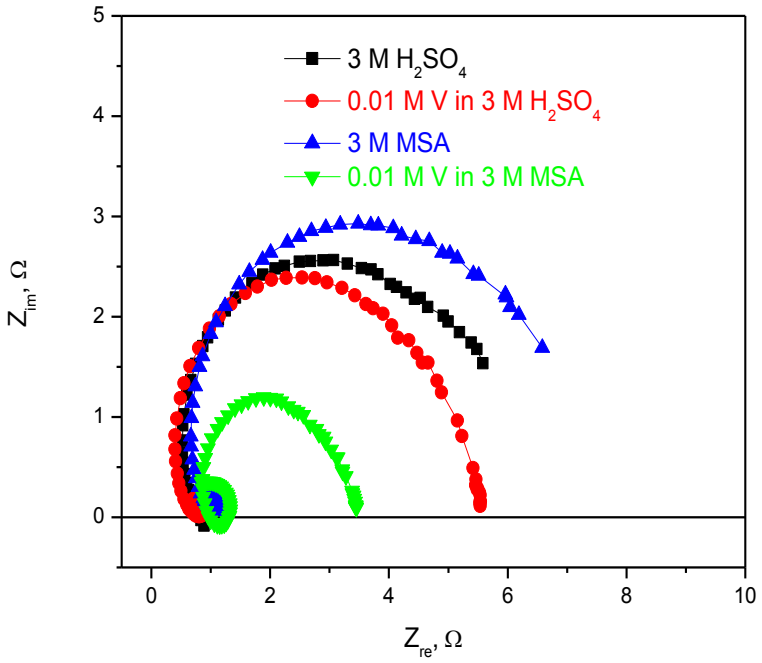

Figure 5-4 Nyquist plots of the test cell using various electrolytes.

The bulk ionic conductivity of various electrolytes is calculated according to the following equation:

$$\sigma = \frac{L}{Z_{re} \cdot A} \quad \text{.....} \quad \text{.....} \quad \text{.....} \quad 5.2$$

wherein:

σ: the ionic conductivity of the electrolyte

L: the overall length of four sensing probes

Z_{re}: ohmic resistance of the cell

A: electrode area available for ionic conduction (width x thickness)

Table 5-1 shows calculated bulk ionic conductivity of various electrolytes using a graphite electrode. All tested electrolytes have very similar ionic conductivity values when they are compared. Compared to pure H_2SO_4, pure MSA has slightly lower bulk ionic conductivity but within the same order of magnitude. This result is consistent with the discovery revealed in the literature.[65, 69] Besides, the bulk ionic conductivity of both electrolytes increases after vanadium ions were added in the solution, which is due to the enhanced ionic strength due to additional vanadium ions in both acid.

Table 5-1 Calculated ionic conductivity of various electrolytes.

Electrolytes	Ohmic Resistance (Ω)	Conductivity (S/cm)
3 M H_2SO_4	0.9487	5.8972
0.01 M V in 3 M H_2SO_4	0.8149	6.8655
3 M MSA	1.1158	5.0141
0.01 M V in 3 M MSA	0.9621	5.8151

5.4 Electrochemical Impedance Spectroscopy Study

EIS was also employed to investigate reaction kinetics and mechanism on MSA based electrolytes given our previous success.[70] Figure 5-5 represents (A) Nyquist plot and (B) Bode plot of a TiO_2 photoelectrode in various electrolytes under AM 1.5 illumination. As seen in Figure 5-5A, one semi-circle at high frequency and one arc/partial arc at mid frequency were observed in all tested electrolytes. The semi-circle corresponds to electron transport resistance and interfacial capacitance at Pt/electrolyte while the arc/partial arc represents charge transfer resistance and interfacial capacitance at TiO_2/vanadium(IV) redox interface. It is clear that all electrolyte has little influence on

electron transport resistance and interfacial capacitance at Pt/electrolyte interface as they all show very similar value near 50 Ω of the real resistance.

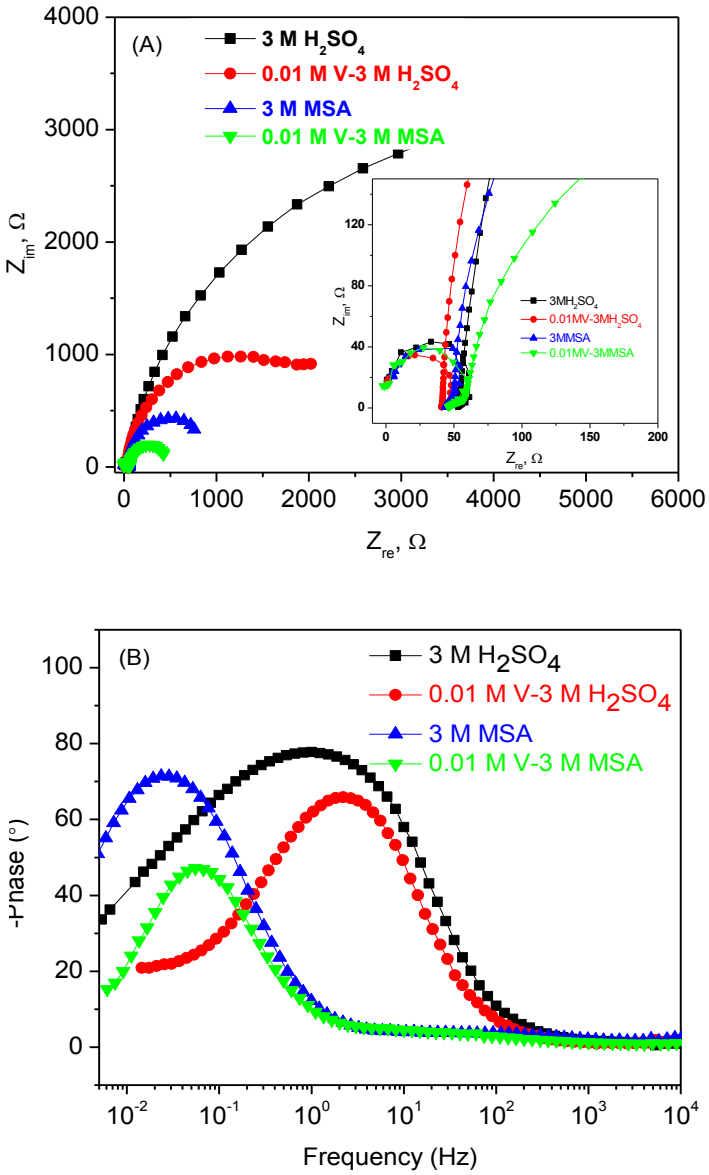

Figure 5-5 Electrochemical impedance spectroscopy of a PEC in the form of (A) Nyquist plot and (B) Bode plot using TiO_2 as the photoelectrode in various electrolytes under AM 1.5 illumination.

However, big difference is seen at the TiO_2/electrolyte interface depending on the selection of electrolyte. 3 M H_2SO_4 electrolyte shows the mid frequency arc with the biggest diameter compared to other three even under AM 1.5 illumination, this is an indicative of slow kinetics of water splitting reactions. After vanadium redox is involved in the electrolyte, charge transfer resistance and interfacial capacitance at the TiO_2/electrolyte interface is reduced greatly due to fast reaction kinetics of vanadium redox, similar as revealed in our previous work.[36, 43, 70] The same argument can be applied to MSA electrolyte as well. Other than that, both MSA-based electrolytes exhibit much smaller charge transfer resistance and interfacial capacitance than H_2SO_4-based electrolytes regardless of vanadium redox participation at TiO_2/electrolyte interface. The 0.01 M V in 3 M MSA electrolyte especially, displays approximate 5 time smaller resistance compared to 0.01 M V in 3 M H_2SO_4. These results are in great agreement with the CV and ZRA results, further proving that MSA holds a great potential as an encouraging electrolyte in photoelectrochemical solar energy conversion and storage.

Figure 5-5B shows Bode plots of a PEC using TiO_2 as the photoelectrode in various electrolytes under AM 1.5 illumination, which is capable of providing lifetime information of the photogenerated electrons in the reaction (calculated according to the following equation and listed in Table 5-2)

$$\tau_e = \frac{1}{2\pi f_{max}} \text{.....5.3}$$

Wherein:

τ_e: the lifetime of electrons

f_{max}: the maximum frequency of the peak in the low frequency region

Clear difference from all electrolytes is seen in Figure 5-5B. Peaks given by two MSA-based electrolytes in despite of vanadium redox, both shift to lower frequency region by two orders of magnitude compared to their counterparts in H_2SO_4 electrolyte as

shown in Table 5-2. This indicates the photoelectron lifetime in MSA-based electrolyte is significantly prolonged compared to H_2SO_4-based electrolytes. This result is in good alignment with our previous CV and ZRA results, indicating a diminished charge carrier recombination and much higher photocatalytic property because of the MSA electrolyte, especially in the presence of vanadium redox species. However, vanadium redox seems to play a negative role in TiO_2 photoelectrode by reducing photoelectron lifetime of TiO_2 photoelectrode and this is true for both H_2SO_4 and MSA acid as the supporting electrolyte. The ratios of photoelectron lifetime in vanadium-acid electrolyte to it in pure acid electrolyte under both H_2SO_4 and MSA circumstances are calculated to be 0.45 and 0.43, which is very close to unity, indicating the same electrochemical and/or photoelectrochemical behavior of vanadium redox in two different acids.

Now one question that needs to be answered is why the vanadium-based electrolyte show much higher photocurrent than pure acid electrolyte regardless of the acid kind whereas its electron lifetime profile exhibits the opposite trend. This is attributed to the quick charge carriers scavenging effect of vanadium redox species due to its fast reaction kinetics. The ratios of electron lifetime in vanadium-acid electrolyte to it in pure acid electrolyte regardless of the supporting electrolyte kind closing to a unity, as indicated earlier, is a strong evidence to indicate the same electrochemical and/or photoelectrochemical behavior of vanadium redox species and to support such speculation. These significantly scavenged charge carriers contribute greatly to the photocurrent. Therefore, although electron lifetime of TiO_2 electrode is shortened vastly in vanadium-based electrolyte compare to pure acid electrolyte, fast reaction kinetics of vanadium species still outperforms such negative effect as indicated in all our previous studies[36, 43, 70] and thus still rendering higher photocurrent as demonstrated in Figure 5-2 and Figure 5-3.

Table 5-2 The maximum frequency of the peak and calculated electron lifetime of a TiO_2 photoelectrode in various electrolytes under AM 1.5 illumination.

Electrolytes	f_{max} (Hz)	τ_e (ms)
3 M H_2SO_4	1	159.2
0.01 M V in 3 M H_2SO_4	2.205	72.2
3 M MSA	0.0235	6775.9
0.01 M V in 3 M MSA	0.055	2895.2

5.5 Long-term Stability Study

Furthermore, the long-term chemical stability of our all-vanadium PEC was studied by conducting photoelectrochemical experiments for prolonged period of time and examining the electrode before and after the experiment. Figure 5-6 illustrates the long-term photoelectrochemical behavior of our all-vanadium PEC using the TiO_2 photoelectrode in 0.01 M V-3 M MSA electrolyte under AM 1.5 illumination for 60 hrs. The cell shows very stable photocurrent throughout the whole test window although slight fluctuation caused by intentional interruption of the light is seen. The photocurrent retention remains 89.5% even after 60 hrs operation. The photocurrent loss may be due to slight concentration loss of vanadium redox species in the photoelectrode during the test. Besides, trivial photoelectrode physical destruction from FTO may also contribute to the loss as slight delamination of TiO_2 was observed after examining the surface of FTO substrate. Judging by our electrode fabrication procedure, our photoelectrode is more a coating rather than a thin film and when the solid is immersed in the liquid for as long as 60 hrs, partial delaminating occurs naturally as the liquid electrolyte tends to swell the solid. This mild electrode physical destruction can be improved by more advanced thin film fabrication techniques, such as electrochemical deposition, chemical vapor deposition (CVD), pulsed laser deposition (PLD) or physical vapor deposition (PVD) etc.

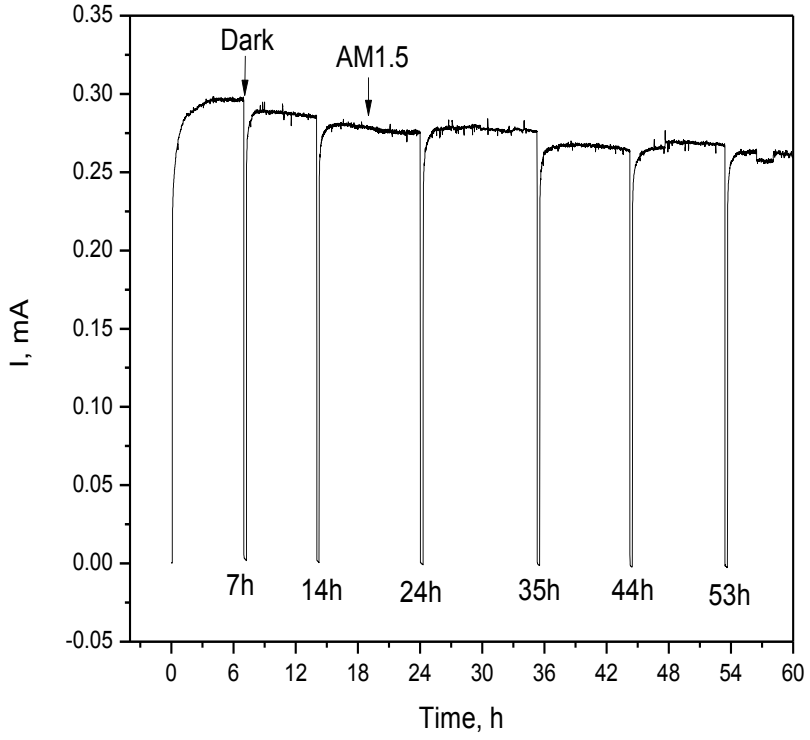

Figure 5-6 Long-term photoelectrochemical profile of all-vanadium PEC using the TiO_2 photoelectrode immersed in 0.01 M V-3 M MSA electrolytes under AM 1.5 illumination for 60 hrs.

XRD was performed on TiO_2 photoelectrode to see any crystal structure/phase change or impurity associated with the photoelectrochemical test and the result is shown in Figure 5-7. It is clearly seen that the crystal structure of TiO_2 remains the same. Only anatase and rutile phase TiO_2 are observed and no impurity detectable is discovered though the intensity of the electrode diminishes a little after long-term test. This is in agreement with observed partial electrode delamination from FTO as the fewer amount of TiO_2 tends to give relatively lower intensity on XRD.

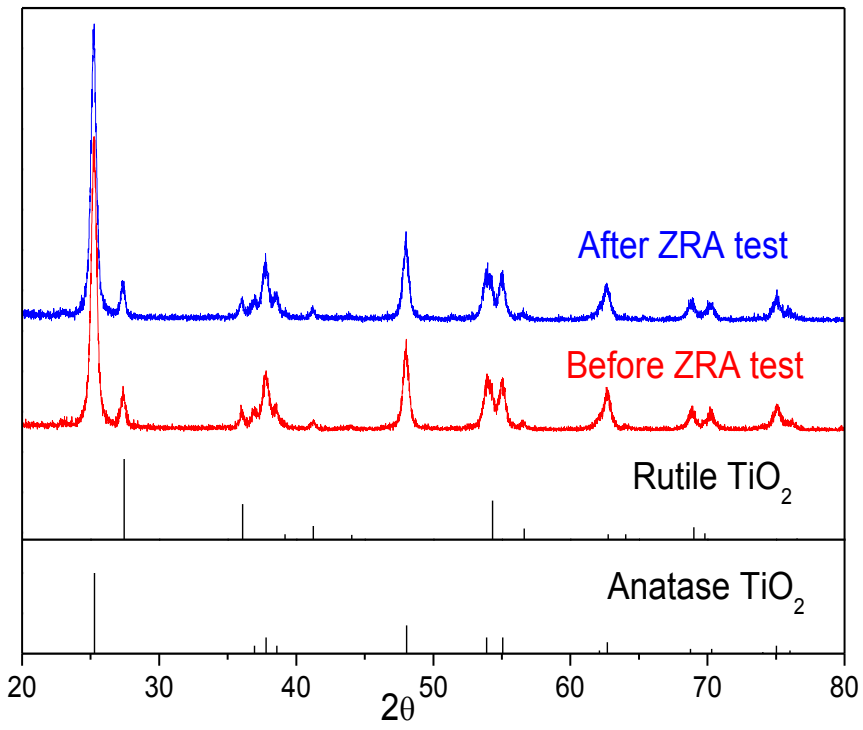

Figure 5-7 XRD spectra of TiO_2 photoelectrode before and after 60 hrs cell operation.

5.6 Efficiencies Measurement

So far, all our experiments have demonstrated improved photocatalytic property for the all-vanadium PEC employing vanadium redox species in the electrolyte. However, these measurements were conducted qualitatively and thus comprehensive study to further quantify the electrode, electrolyte and the system is needed. Herein, characteristic measurements of all-vanadium PEC such as Faradaic efficiency, incident photo-to-current conversion efficiency (IPCE) of the PEC were implemented to reveal its photoelectrochemical performance quantitatively.

Recently, UV-vis spectroscopy has been developed[72-75] to monitor state of charge of all-vanadium redox batteries, such method was also utilized in our study to

monitor the electrolyte concentration change while the all-vanadium PEC was in operation. Figure 5.8 shows the concentration change of vanadium(IV, VO^{2+}) ions at the beginning, in the middle and the end of the 60 hrs photocharging process as demonstrated in Figure 5-6. As the photocharging process proceeds, the vanadium(IV) ions concentration starts to decrease, indicating more and more VO^{2+} ions are converting to VO^{+} ions by photogenerated charge carriers, i.e., holes, in the anolyte chamber.

To calculate Faradaic efficiency of the PEC, the light was blocked intentionally at certain period of time during the test and a small amount (~10 ml) of the electrolyte in a quartz cuvette with 1 cm path length was analyzed using a UV–vis spectrophotometer (PerkinElmer Lambda 35) to determine the electrolyte concentration change.

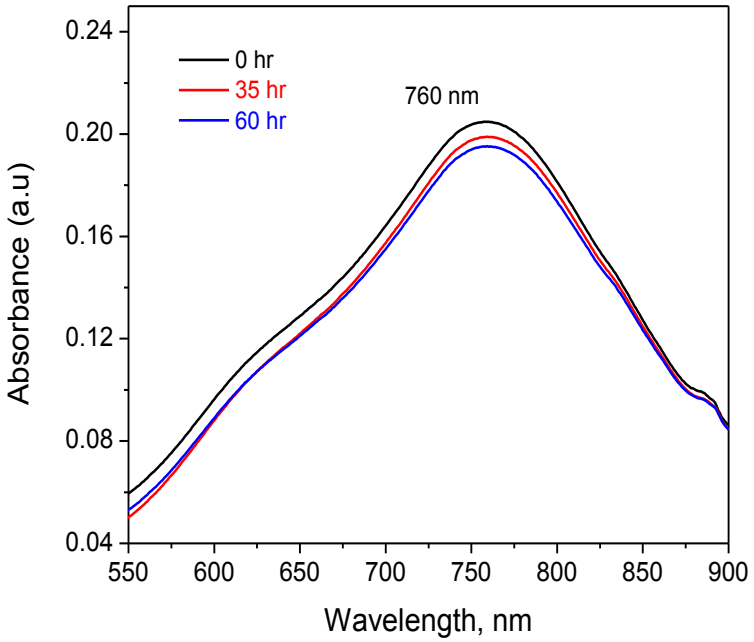

Figure 5-8 UV-vis absorbance spectra of 0.01 M vanadium(IV) ions in 3 M MSA electrolyte at different period of time of photocharging.

According to Beer-Lambert law, i.e.,

$$A = \varepsilon lc \text{.....5.4}$$

Where:

ε (L· mol^{-1}· cm^{-1}): molar absorptivity of the sample measured

l (cm): the path length of the cuvette in which the sample is contained

c (mol/L^{-1}): the concentration of the compound in solution

The Faradaic efficiency (η_F), defined as the following equation

$$\eta_F = \frac{F \cdot \Delta n}{\Delta Q} \text{ .....5.5}$$

Wherein:

Δn: the amount of reacted VO^{2+} during the photocharging process

F: the Faraday's constant as 96485 C/mol

ΔQ: the charge transferred during the photocharging process

is then calculated to be 84.8%.

To measure the incident photon-to-current conversion efficiency (IPCE) of the cell, the wavelength of the incident light was controlled by a monochromator (Optometrics) from 200 nm to 600 nm, then the IPCE was calculated according to the following equation:[44]

$$IPCE = \frac{1240 \cdot I_{ph}}{\lambda \cdot J_{light}} \text{ .....5.6}$$

Wherein:

I_{ph} (A/cm^2): the measured photocurrent density at a specific wavelength

λ (nm): the wavelength of incident light

J_{light} (W/cm^2): the light irradiance determined by a photodetector (Newport, USA)

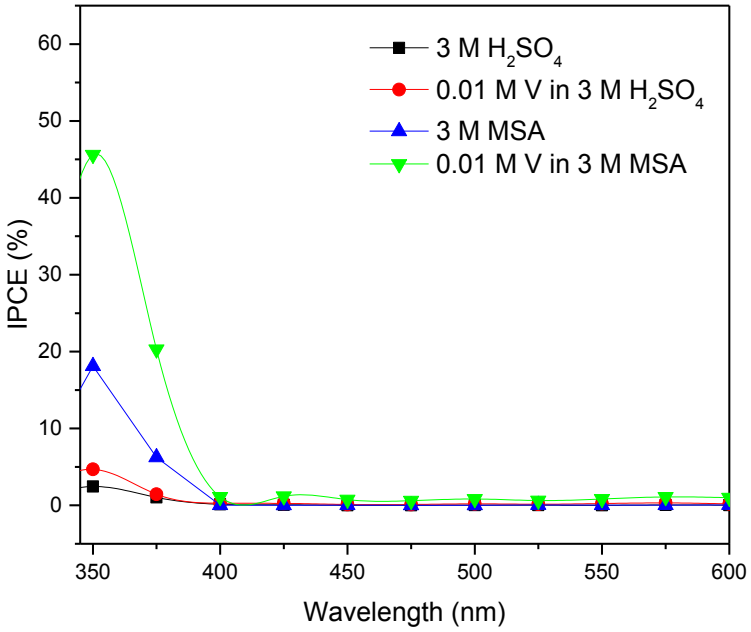

Figure 5-9 IPCE of the PEC using a TiO_2 photoelectrode in various electrolytes.

The incident photon-to-current efficiency (IPCE) of the PEC storage cell using various electrolytes is shown in Figure 5-9. The results are in agreement with our previous work[44] and the findings observed in chapter 5. All curves show a maximum efficiency at 350 nm regardless of the electrolyte, which indicates the large bandgap of TiO_2 that only absorbs light in UV region. Pure H_2SO_4 electrolyte only gives a low IPCE value as 2.45% due to slow reaction kinetics of water splitting reaction whereas pure MSA electrolyte improves cell IPCE more than 7 times compared to the former. On the other hand, vanadium redox as expected, plays a significant role by boosting IPCE of the cell, especially with MSA electrolyte. With vanadium redox in the electrolyte, IPCE of the cell is doubled for sulfuric acid. When sulfuric acid is replaced with MSA as the supporting electrolyte, the highest value (45.6%) is achieved with the assistance of vanadium redox, improving IPCE of the cell by a factor of 18.6, 9.7, and 2.5 compared to

pure H_2SO_4 acid, 0.01 M V in 3 M H_2SO_4 and pure MSA electrolyte respectively. Such huge enhancement on IPCE of the cell is believed due to synergy between fast vanadium redox kinetics and prolonged electron life time of MSA.

5.7 Conclusion

In this chapter, we investigated the electrochemical and photoelectrochemical performance, ionic conductivity, chemical stability, reaction kinetics of vanadium redox species in MSA electrolyte by CV, ZRA and EIS.

CV results show that MSA is chemically stable within large potential window tested from -0.5 to 2.1 V under either dark or AM 1.5 illumination. The photocurrent is extensively boosted in MSA-based electrolyte compared to H_2SO_4-based electrolyte according to both CV and ZRA measurements, especially in the presence of vanadium redox species.

Although the ionic conductivity of MSA is found closely comparable to that of conventional strong acid as H_2SO_4 under same concentration regardless of the involvement of vanadium redox species however, EIS Nyquist plots reveal that MSA is capable of diminishing charge transfer resistance and interfacial capacitance at photoelectrode/electrolyte interface under AM 1.5 illumination, especially when vanadium redox species participates in the reaction. Other than that, EIS Bode plots manifest that much higher electron lifetime is realized on MSA-based electrolytes in photoelectrochemical reactions compare to H_2SO_4-based electrolytes. In addition, the fast reaction kinetics of vanadium redox species shortens electron lifetime of the TiO_2 photoelectrode in both acids greatly due to their quick charge scavenging ability.

The long-term (60 hrs) chemical stability measurement of all-vanadium PEC reveals rather stable photoelectrochemical behavior of the system and XRD

characterization conducted on TiO_2 photoelectrode shows no crystal structural change of the material.

The cell properties, such as Faradaic efficiency and IPCE were investigated at last. The vanadium redox species concentration is discovered to reduce after long-term photocharging experiment and the Faradaic efficiency of the PEC is calculated to be 84.8%. IPCE of the PEC were collected using the TiO_2 photoelectrode in various electrolytes and the results match well with our previous CV, ZRA and EIS findings in chapter 5. The highest IPCE of the PEC 45.6%, was achieved on 0.01 M V-3 M MSA electrolyte and is attributed to the synergistic effect of fast reaction kinetics of vanadium redox and prolonged electron life time of MSA.

Chapter 6

Conclusion

Photoelectrochemical cell (PEC) is an electrochemical device that provides a practical means of transforming solar energy into electricity or chemical fuels such as H_2 upon solar illumination. However, low solar-to-hydrogen conversion efficiency, lack of cost-effective approaches to continuously produce H_2 fuel regardless of the intermittent nature of the sun slight and the very low energy density of hydrogen gas at ambient conditions serve as a few greatest hurdles in advancing this promising technique in last four decades.

In this study, an all-vanadium PEC was proposed and developed, and its electrochemical and photoelectrochemical performance was investigated using common photoelectrodes such as TiO_2 and WO_3/TiO_2 hybrid electrodes via multiple instrumental and electrochemical methods.

The proof-of-the-concept experiment conducted on TiO_2 electrode clearly reveals a significant photoresponse enhancement compared to photolysis of water and even higher photocurrent on the WO_3/TiO_2 hybrid electrode in contact with one vanadium redox pair. Further photoelectrochemical study using the WO_3/TiO_2 hybrid electrode shows more remarkably enhanced photocurrent when two pairs of vanadium redox couples were employed in an all-vanadium photoelectrochemical cell.

It is believed that the vanadium redox pairs serve two purposes in the electrochemical and/or photoelectrochemical reactions: (i) quickly scavenge the charge carriers, mitigate their recombination and thus boost the photocurrent, and (ii) shift the dynamic equilibrium between charge carrier recombination and redox reaction toward the latter due to fast kinetics of these vanadium redox couples.

In addition, a photocharge/discharge process was discovered on WO_3-based electrodes due to the formation/decomposition of hydrogen tungsten bronze (H_xWO_3) under irradiation in highly acidic environment regardless of vanadium redox reactions. CV and ZRA results reveal greatly mitigated photocurrent in pure acid electrolyte but enhanced photoresponse of the hybrid electrode in all-vanadium electrolytes. Without applying the bias, hydrogen tungsten bronze was formed in both pure acid and all-vanadium electrolytes, and this finding was corroborated by EIS results, material characterization results and proposed mechanism model. In pure acid, the formed hydrogen tungsten bronze acts as the hurdle to prevent electron transport and thus mitigates the photocurrent; whereas the all-vanadium electrolytes are beneficial to revitalize photocurrent of the hybrid electrodes under illumination and render energy storage ability under dark. In light of such a synergy effect, the alliance of vanadium redox reaction and WO_3/TiO_2 hybrid electrode would potentially enable a unique dual solar/electron storage system albeit the intermittent nature of sunlight.

To optimize the cell, the existing supporting electrolyte sulfuric acid was replaced with methanesulfonic acid (MSA) to realize better photocatalytic property of the all-vanadium PEC. CV, ZRA and conductivity measurements show that MSA is a chemically stable supporting electrolyte with conductivity comparable to conventional sulfuric acid but rendering much higher photoelectrochemical performance and therefore higher efficiency. According to EIS results, such ability of MSA compare to H_2SO_4-based electrolytes, is rooted from its prolonged electron lifetime and being capable of diminishing charge transfer resistance and interfacial capacitance at photoelectrode/electrolyte interface under AM 1.5 illumination, especially when vanadium redox species participates in the reaction.

Although electron lifetime of the TiO_2 photoelectrode is shortened greatly in both acids with the involvement of vanadium redox species, the fast reaction kinetics of vanadium redox species plays the key role in achieving remarkable photoresponse and cell efficiencies due to their quick charge scavenging ability.

Appendix

Achievements

During my PhD study in Department of Materials Science and Engineering at University of Texas at Arlington, all achievements were made and reflected in the following public exposures, journals, patents and conferences.

PUBLIC EXPOSURE (examples):

UTA homepage UTA Shorthorn Science Daily Science Newsline

News codex American Laboratory Kurzweil News

JOURNALS:

1. **Dong Liu**, Zi Wei et al, Reversible Electron Storage in an All-Vanadium Photoelectrochemical Storage Cell: Synergy between Vanadium Redox and Hybrid Photocatalyst, 2015, **ACS Catalysis**, 5, 2632-2639
2. **Dong Liu**, Zi Wei et al, Efficient Solar Energy Storage Using A TiO_2/WO_3 Tandem Photoelectrode in An All-vanadium Photoelectrochemical Cell, **Electrochimica Acta**, 2014, 136, 435-441
3. **Dong Liu**, Fuqiang Liu et al, Effect of Vanadium Redox Species on Photoelectrochemical Behavior of TiO_2 and TiO_2/WO_3 Photo-electrodes, **Journal of Power Sources**, 2012, 213, 78-82
4. **Dong Liu**, Zi Wei et al, Ultra-long Electron Lifetime Induced Efficient Solar Energy Storage by an All-Vanadium Photoelectrochemical Storage Cell Using Methanesulfonic Acid, **Journal of Materials Chemistry A,** under review
5. Zi Wei, **Dong Liu** et al, All-vanadium Redox Photoelectrochemical Cell: An Approach to Store Solar Energy, **Electrochemistry Communications**, 2014, 45, 79-82

6. Zi Wei, **Dong Liu** et al, Carbon Coated TiO_2 Photoanode for All-vanadium Redox Photoelectrochemical Cell as Efficient Solar Energy Storage Device, **ECS Transaction**, 2015, In press
7. Zi Wei, Yi Shen, **Dong Liu** et al, Improved Solar Energy Storage Efficiency of All-Vanadium Photoelectrochemical Cell using Geometry-Enhanced TiO_2 Nanobelts, **ACS Nano**, under review
8. Syed Dawar Sajjad, **Dong Liu** et al, Guanidinium Based Blend Anion Exchange Membranes for Direct Methanol Alkaline Fuel Cells (DMAFCs), **Journal of Power Sources**, 2015, In press
9. Chiajen Hsu, Shen Yi, Zi Wei, **Dong Liu** et al, Anatase TiO_2 Nanobelts with Plasmonic Au Decoration Exhibiting Efficient Charge Separation and Enhanced Activity, **Journal of Alloys and Compounds**, 2014, 613, 117-121
10. Noor Siddique, Amir Salehi, Zi Wei, **Dong Liu** et al., Length-scale Dependent Phase Transformation of $LiFePO_4$: An In situ and Operando Study Using Micro Raman Spectroscopy and XRD, **ChemPhysChem**, 2015, accepted, DOI: 10.1002/cphc.201500299R1

PATENTS:

1. Fuqiang Liu (advisor), **Dong Liu**, Wei Zi, Yi Shen, A Continuous Flow Reactor for Highly Efficient Regenerative Solar Energy Storage using Vanadium Redox, **U.S. Patent**, 2015, appl. No: 62/162,976

CONFERENCES:

1. **Dong Liu**, Fuqiang Liu, Regenerative Solar Energy Storage via Photocatalytic Redox Reaction, **The 221st ECS Conference**, 2012, Seattle, WA

2. **Dong Liu**, Fuqiang Liu, Photo-assisted energy storage via Vanadium(IV) Redox species, **ASM Symposium of North Texas Inter-University**, 2012, Denton, TX
3. Zi Wei, **Dong Liu** et al, An Efficient Solar Energy Storage System: All Vanadium Redox Photoelectrochemical Cell, **The 227th ECS Conference**, 2015, Chicago, IL
4. Zi Wei, **Dong Liu**, Yi Shen, et al., Enhanced Photoactivity Using TiO_2 Nanobelts in An All Vanadium Redox Photoelectrochemical Cell, **The 50th anniversary TSM meeting**, 2015, Austin, TX
5. Zi Wei, **Dong Liu** et al., All-vanadium Redox Photo-electrochemical Cell: An New Approach to Store Solar Energy, **The 49th anniversary TSM meeting**, 2014, Arlington, TX

References

[1] N.S. Lewis, Toward Cost-Effective Solar Energy Use, Science, 315 (2007) 798.

[2] M. Wolf, Solar Energy Utilization by Physical Methods, Science, 184 (1974) 382.

[3] G.C. Nathan S. Lewis, Arthur J. Nozik, Michael R. Wasielewski, Paul Alivisatos, Basic research needs for solar energy ultilization, 2005, pp. 276.

[4] N.S. Lewis, Artificial photosynthesis, American Scientist, 83 (1995) 534.

[5] M. Gratzel, Photoelectrochemical cells, Nature, 414 (2001) 338.

[6] R.N. Pandey, K.S.C. Babu, O.N. Srivastava, High conversion efficiency photoelectrochemical solar cells, Progress in Surface Science, 52 (1996) 125.

[7] A. Fujishima, K. Honda, Electrochemical Photolysis of Water at a Semiconductor Electrode, Nature, 238 (1972) 37.

[8] A.J. Bard, Photoelectrochemistry, Science, 207 (1980) 139.

[9] A. Heller, Conversion of sunlight into electrical power and photoassisted electrolysis of water in photoelectrochemical cells, Accounts of Chemical Research, 14 (1981) 154.

[10] Y.V. Pleskov, Solar energy conversion in photoelectrochemical cells with semiconductor electrodes, Progress in Surface Science, 15 (1984) 401.

[11] K. Rajeshwar, P. Singh, J. DuBow, Energy conversion in photoelectrochemical systems — a review, Electrochimica Acta, 23 (1978) 1117.

[12] M.G. Walter, E.L. Warren, J.R. McKone, S.W. Boettcher, Q. Mi, E.A. Santori, N.S. Lewis, Solar Water Splitting Cells, Chemical Reviews, 110 (2010) 6446.

[13] O.V. Craig Grimes, Sudhir Ranjan, Light, Water, Hydrogen-The Solar Generation of Hydrogen by Water Photoelectrolysis, Springer US2008.

[14] S. Licht, G. Hodes, R. Tenne, J. Manassen, A light-variation insensitive high efficiency solar cell, Nature, 326 (1987) 863.

[15] S. Licht, Photoelectrochemical Storage Cell, Photoconversion of Solar Energy, World Scientific Publishing Co, 2008.

[16] G. Hodes, D. Cohen, J. Manassen, Photoelectrochemical cells, Chemtech, 11 (1981) 112.

[17] K. Fujihara, T. Ohno, M. Matsumura, Splitting of water by electrochemical combination of two photocatalytic reactions on TiO_2 particles, Journal of the Chemical Society, Faraday Transactions, 94 (1998) 3705.

[18] S. Licht, Photoelectrochemical Solar Energy Storage Cells, Encyclopedia of Electrochemistry, Wiley-VCH Verlag GmbH & Co, 2007.

[19] C.-C. Lo, C.-W. Huang, C.-H. Liao, J.C.S. Wu, Novel twin reactor for separate evolution of hydrogen and oxygen in photocatalytic water splitting, International Journal of Hydrogen Energy, 35 (2010) 1523.

[20] T. Ohno, D. Haga, K. Fujihara, K. Kaizaki, M. Matsumura, Unique Effects of Iron(III) Ions on Photocatalytic and Photoelectrochemical Properties of Titanium Dioxide, The Journal of Physical Chemistry B, 101 (1997) 6415.

[21] S.-C. Yu, C.-W. Huang, C.-H. Liao, J.C.S. Wu, S.-T. Chang, K.-H. Chen, A novel membrane reactor for separating hydrogen and oxygen in photocatalytic water splitting, Journal of Membrane Science, 382 (2011) 291.

[22] T. Simon, N. Bouchonville, M.J. Berr, A. Vaneski, A. Adrović, D. Volbers, R. Wyrwich, M. Döblinger, A.S. Susha, A.L. Rogach, F. Jäckel, J.K. Stolarczyk, J. Feldmann, Redox shuttle mechanism enhances photocatalytic H_2 generation on Ni-decorated CdS nanorods, Nat Mater, 13 (2014) 1013.

[23] N.A. Ramos-Delgado, M.A. Gracia-Pinilla, L. Maya-Treviño, L. Hinojosa-Reyes, J.L. Guzman-Mar, A. Hernández-Ramírez, Solar photocatalytic activity of TiO_2

modified with WO_3 on the degradation of an organophosphorus pesticide, Journal of Hazardous Materials, 263, Part 1 (2013) 36.

[24] I. Shiyanovskaya, M. Hepel, Bicomponent WO_3/TiO_2 Films as Photoelectrodes, Journal of The Electrochemical Society, 146 (1999) 243.

[25] N.R. de Tacconi, C.R. Chenthamarakshan, G. Yogeeswaran, A. Watcharenwong, R.S. de Zoysa, N.A. Basit, K. Rajeshwar, Nanoporous TiO_2 and WO_3 Films by Anodization of Titanium and Tungsten Substrates: Influence of Process Variables on Morphology and Photoelectrochemical Response, The Journal of Physical Chemistry B, 110 (2006) 25347.

[26] S. Higashimoto, T. Shishido, Y. Ohno, M. Azuma, M. Takahashi, M. Anpo, Photocharge-Discharge Behaviors of Hybrid WO_3/TiO_2 Film Electrodes: Conversion, Storage of Electrons, and the Effect of the WO_3 Structure on Rechargeability, Journal of The Electrochemical Society, 154 (2007) F48.

[27] A.J. Bard, Photoelectrochemistry and heterogeneous photo-catalysis at semiconductors, Journal of Photochemistry, 10 (1979) 59.

[28] N. Getoff, Photoelectrochemical and photocatalytic methods of hydrogen production: A short review, International Journal of Hydrogen Energy, 15 (1990) 407.

[29] Y.Y.G. Yu. V. Pleskov, Semiconductor Photoelectrochemistry, Springer, 2012.

[30] R.P. Allen J. Bard, Joseph Jordan, Standard Potentials in Aqueous Solution, CRC Press, 1985.

[31] M. Gattrell, J. Park, B. MacDougall, J. Apte, S. McCarthy, C.W. Wu, Study of the Mechanism of the Vanadium 4+/5+ Redox Reaction in Acidic Solutions, Journal of The Electrochemical Society, 151 (2004) A123.

[32] G. Oriji, Y. Katayama, T. Miura, Investigation on V(IV)/V(V) species in a vanadium redox flow battery, Electrochimica Acta, 49 (2004) 3091.

[33] G. Oriji, Y. Katayama, T. Miura, Investigations on V(IV)/V(V) and V(II)/V(III) redox reactions by various electrochemical methods, Journal of Power Sources, 139 (2005) 321.

[34] L.G. Hepler, J.O. Hill, I.G. Worsley, Thermochemistry and oxidation potentials of vanadium, niobium, and tantalum, Chemical Reviews, 71 (1971) 127.

[35] X. Liu, F. Wang, Q. Wang, Nanostructure-based WO_3 photoanodes for photoelectrochemical water splitting, Physical Chemistry Chemical Physics, 14 (2012) 7894.

[36] D. Liu, F. Liu, J. Liu, Effect of vanadium redox species on photoelectrochemical behavior of TiO_2 and TiO_2/WO_3 photo-electrodes, Journal of Power Sources, 213 (2012) 78.

[37] S. Higashimoto, N. Kitahata, K. Mori, M. Azuma, Photo-electrochemical properties of amorphous WO_3 supported on TiO_2 hybrid catalysts, Catalysis Letters, 101 (2005) 49.

[38] S. Higashimoto, Y. Ushiroda, M. Azuma, Electrochemically Assisted Photocatalysis of Hybrid WO_3/TiO_2 Films: Effect of the WO_3 Structures on Charge Separation Behavior, Topics in Catalysis, 47 (2008) 148.

[39] T. Tatsuma, S. Saitoh, Y. Ohko, A. Fujishima, TiO_2−WO_3 Photoelectrochemical Anticorrosion System with an Energy Storage Ability, Chemistry of Materials, 13 (2001) 2838.

[40] C. Ng, A. Iwase, Y.H. Ng, R. Amal, Understanding Self-Photorechargeability of WO_3 for H_2 Generation without Light Illumination, ChemSusChem, 6 (2013) 291.

[41] C. Ng, Y.H. Ng, A. Iwase, R. Amal, Visible light-induced charge storage, on-demand release and self-photorechargeability of WO_3 film, Phys Chem Chem Phys, 13 (2011) 13421.

[42] P. Ngaotrakanwiwat, T. Tatsuma, S. Saitoh, Y. Ohko, A. Fujishima, Charge-discharge behavior of TiO_2-WO_3 photocatalysis systems with energy storage ability, Physical Chemistry Chemical Physics, 5 (2003) 3234.

[43] D. Liu, Z. Wei, C.-j. Hsu, Y. Shen, F. Liu, Efficient Solar Energy Storage Using A TiO_2/WO_3 Tandem Photoelectrode in An All-vanadium Photoelectrochemical Cell, Electrochimica Acta, 136 (2014) 435.

[44] Z. Wei, D. Liu, C. Hsu, F. Liu, All-vanadium redox photoelectrochemical cell: An approach to store solar energy, Electrochemistry Communications, 45 (2014) 79.

[45] P.G. Dickens, M.S. Whittingham, The tungsten bronzes and related compounds, Quarterly Reviews, Chemical Society, 22 (1968) 30.

[46] D. Yoon, A. Manthiram, Hydrogen tungsten bronze as a decoking agent for long-life, natural gas-fueled solid oxide fuel cells, Energy & Environmental Science, 7 (2014) 3069.

[47] M.S. Whittingham, Hydrogen motion in oxides: from insulators to bronzes, Solid State Ionics, 168 (2004) 255.

[48] P.J. Wiseman, P.G. Dickens, The crystal structure of cubic hydrogen tungsten bronze, Journal of Solid State Chemistry, 6 (1973) 374.

[49] L. Wang, L. Yuan, X. Wu, J. Wu, C. Hou, S. Feng, Electrochromic response of pulsed laser deposition prepared WO_3-TiO_2 composite film, RSC Advances, 4 (2014) 47670.

[50] I. Paramasivam, Y.-C. Nah, C. Das, N.K. Shrestha, P. Schmuki, WO_3/TiO_2 Nanotubes with Strongly Enhanced Photocatalytic Activity, Chemistry – A European Journal, 16 (2010) 8993.

[51] Y.R. Ahn, C.R. Park, S.M. Jo, D.Y. Kim, Enhanced charge-discharge characteristics of RuO_2 supercapacitors on heat-treated TiO_2 nanorods, Applied Physics Letters, 90 (2007) 122106.

[52] I. Abayev, A. Zaban, F. Fabregat-Santiago, J. Bisquert, Electronic conductivity in nanostructured TiO_2 films permeated with electrolyte, physica status solidi (a), 196 (2003) R4.

[53] L.R.F. Allen J. Bard, Electrochemical Methods: Fundamentals and Applications, Wiley2000.

[54] G. Hodes, D. Cahen, J. Manassen, Tungsten trioxide as a photoanode for a photoelectrochemical cell (PEC), Nature, 260 (1976) 312.

[55] L. Vayssieres, On Solar Hydrogen and Nanotechnology, Wiley2010.

[56] O. Khaselev, J.A. Turner, A Monolithic Photovoltaic-Photoelectrochemical Device for Hydrogen Production via Water Splitting, Science, 280 (1998) 425.

[57] P.P. González-Borrero, F. Sato, A.N. Medina, M.L. Baesso, A.C. Bento, G. Baldissera, C. Persson, G.A. Niklasson, C.G. Granqvist, A. Ferreira da Silva, Optical band-gap determination of nanostructured WO_3 film, Applied Physics Letters, 96 (2010) 061909.

[58] L. Yang, H. Zhou, T. Fan, D. Zhang, Semiconductor photocatalysts for water oxidation: current status and challenges, Physical Chemistry Chemical Physics, 16 (2014) 6810.

[59] X. Lu, S. Xie, H. Yang, Y. Tong, H. Ji, Photoelectrochemical hydrogen production from biomass derivatives and water, Chemical Society Reviews, 43 (2014) 7581.

[60] C. Tang, D. Zhou, Methanesulfonic acid solution as supporting electrolyte for zinc-vanadium redox battery, Electrochimica Acta, 65 (2012) 179.

[61] P.K. Leung, M.R. Mohamed, A.A. Shah, Q. Xu, M.B. Conde-Duran, A mixed acid based vanadium–cerium redox flow battery with a zero-gap serpentine architecture, Journal of Power Sources, 274 (2015) 651.

[62] N.-F.W. Sui Peng, Xiao-Juan Wu, Su-Qin Liu, Dong Fang, You-Nian Liu, Ke-Long Huang, Vanadium Species in CH_3SO_3H and H_2SO_4 Mixed Acid as the Supporting Electrolyte for Vanadium Redox Flow Battery, International Journal of Electrochemical Science, 7 (2012) 643.

[63] Z. He, Z. Li, Z. Zhou, F. Tu, Y. Jiang, C. Pan, S. Liu, Improved performance of vanadium redox battery using methylsulfonic acid solution as supporting electrolyte, Journal of Renewable and Sustainable Energy, 5 (2013) 023130.

[64] G. Wang, J. Chen, X. Wang, J. Tian, H. Kang, X. Zhu, Y. Zhang, X. Liu, R. Wang, Study on stabilities and electrochemical behavior of V(V) electrolyte with acid additives for vanadium redox flow battery, Journal of Energy Chemistry, 23 (2014) 73.

[65] R. Solarska, R. Jurczakowski, J. Augustynski, A highly stable, efficient visible-light driven water photoelectrolysis system using a nanocrystalline WO_3 photoanode and a methane sulfonic acid electrolyte, Nanoscale, 4 (2012) 1553.

[66] M. Zukalova, M. Bousa, Z. Bastl, I. Jirka, L. Kavan, Electrochemical Doping of Compact TiO_2 Thin Layers, The Journal of Physical Chemistry C, 118 (2014) 25970.

[67] T. Berger, T. Lana-Villarreal, D. Monllor-Satoca, R. Gómez, Charge transfer reductive doping of nanostructured TiO_2 thin films as a way to improve their photoelectrocatalytic performance, Electrochemistry Communications, 8 (2006) 1713.

[68] H. Pelouchova, P. Janda, J. Weber, L. Kavan, Charge transfer reductive doping of single crystal TiO_2 anatase, Journal of Electroanalytical Chemistry, 566 (2004) 73.

[69] M. D. Gernon, M. Wu, T. Buszta, P. Janney, Environmental benefits of methanesulfonic acid . Comparative properties and advantages, Green Chemistry, 1 (1999) 127.

[70] D. Liu, W. Zi, S.D. Sajjad, C. Hsu, Y. Shen, M. Wei, F. Liu, Reversible Electron Storage in an All-Vanadium Photoelectrochemical Storage Cell: Synergy between Vanadium Redox and Hybrid Photocatalyst, ACS Catalysis, 5 (2015) 2632.

[71] M. Vijayakumar, S.D. Burton, C. Huang, L. Li, Z. Yang, G.L. Graff, J. Liu, J. Hu, M. Skyllas-Kazacos, Nuclear magnetic resonance studies on vanadium(IV) electrolyte solutions for vanadium redox flow battery, Journal of Power Sources, 195 (2010) 7709.

[72] Z. Tang, D.S. Aaron, A.B. Papandrew, T.A. Zawodzinski, Monitoring the State of Charge of Operating Vanadium Redox Flow Batteries, ECS Transactions, 41 (2012) 1.

[73] X. Gao, R.P. Lynch, M.J. Leahy, D.N. Buckley, Spectroscopic Study of Vanadium Electrolytes in Vanadium Redox Flow Battery (VRFB), ECS Transactions, 45 (2013) 25.

[74] R.P. Brooker, C.J. Bell, L.J. Bonville, H.R. Kunz, J.M. Fenton, Determining Vanadium Concentrations Using the UV-Vis Response Method, Journal of The Electrochemical Society, 162 (2015) A608.

[75] M. Skyllas-Kazacos, M. Kazacos, State of charge monitoring methods for vanadium redox flow battery control, Journal of Power Sources, 196 (2011) 8822.

Biographical Information

Before coming to United States to pursue a higher education, Dong Liu was born in China and lived most of his life there. He was conferred his Bachelor of Science (BS) degree in Applied Chemistry (Materials Science) from Zhejiang University of Technology in 2004 and his Master of Science (MS) degree in Materials Science and Engineering from East China University of Science and Technology and Auburn University in 2007 and 2010 respectively.

In 2010 he joined The University of Texas at Arlington to pursue his doctoral degree and worked under supervision of Dr. Fuqiang Liu in Department of Materials Science and Engineering and received his Ph.D. degree in 2015. His primary research area during his doctoral study was science, engineering and technology of all-vanadium photoelectrochemical cell, while he also worked on vanadium redox flow battery and lithium-ion battery. His academic achievements within his PhD program were reported in Appendix of this thesis.

He is going to work in either academia or industry to keep strengthening his professional career and plans to become a leader in both technical and managerial roles in next 5 years after graduation.